Title: Blockade of VCAM1 or VLA4 preserves cerebrovasculature and prevents cognitive decline late after stroke

Authors: Kristy A. Zera[1], Karen Bradshaw[1], Li Zhu[1], Oliver Hahn[1], Aulden Foltz[1], Todd Peterson[1,2], Hanadie Yousef[1,3], Davis Lee[1,3], Elizabeth W. Mayne[1,6], Nima Aghaeepour[4,5,6], Tony Wyss-Coray[1,3], Marion S. Buckwalter[1,7]

[1]Department of Neurology and Neurological Sciences, Stanford University School of Medicine, Stanford, CA, USA
[2]Department of Psychology, University of North Carolina Wilmington, Wilmington, NC, USA
[3]VA Palo Alto Health Care System, Palo Alto, CA, USA.
[4]Department of Anesthesiology, Perioperative & Pain Medicine, Stanford University School of Medicine, Stanford, CA, USA
[5]Department of Biomedical Data Sciences, Stanford University School of Medicine, Stanford, CA, USA
[6]Department of Pediatrics, Stanford University School of Medicine, Stanford, CA, USA
[7]Department of Neurosurgery, Stanford University School of Medicine, Stanford University, Stanford, CA, USA

Correspondence may be directed to:
Marion S. Buckwalter, MD PhD
Department of Neurology and Neurological Sciences
Stanford School of Medicine
1201 Welch Rd.
Stanford, CA, 94305-5489
Phone: 650-724-9098
Email: marion.buckwalter@stanford.edu

Conflict of Interest:
Dr. Marion S. Buckwalter has worked as a consultant for Roche, Genentech, and EMD Serrano, unrelated to this project. The remaining authors have declared that no conflict of interest exists.

Abstract:

Infarct-induced neurodegeneration increases dementia risk for at least a decade in humans. It can be modeled in wildtype mice, where a cortical stroke results in chronic lymphocytic infiltration into the infarct and delayed cognitive decline. Vascular cell adhesion molecule 1 (VCAM1) on endothelial cells is increased by stroke and facilitates immune cell diapedesis by binding very late antigen 4 (VLA4) on immune cells. We report here that after stroke, chronic but not acute treatment with a VCAM1 blocking antibody reduces B and T lymphocyte infiltration and prevents chronic cognitive dysfunction in wildtype male and female mice. Preservation of cognitive function also occurred after chronic anti-VLA4 treatment despite anti-VLA4's lack of effect on lymphocyte infiltration. High-depth single-cell RNA sequencing of the chronic infarct and peri-infarct cortex revealed an infarct-induced decrease in expression of blood vessel growth and maturation genes in endothelial cells that was reversed by both anti-VLA4 and anti-VCAM1. Plasma proteomics also support a vasculoprotective mechanism of anti-VCAM1. Finally, immunostaining demonstrated that both antibodies improve pericyte coverage of the vasculature and prevent extravascular fibrinogen leakage. Together, our findings indicate that vascular structure and function remain abnormal long after stroke and that the VLA4/VCAM1 axis is a promising treatment target for infarct-induced neurodegeneration as blockade of either molecule restores cerebrovasculature and prevents cognitive decline.

Introduction:

Cognitive dysfunction is a common and debilitating complication of stroke (1). Stroke independently doubles the risk of subsequent cognitive impairment for at least a decade, irrespective of established vascular dementia risk factors or the occurrence of multiple infarcts over time (1–3). Stroke occurs in over 12.2 million people worldwide each year, and ischemic stroke represents 87% of these cases (4). Cognitive decline affects up to one-third of stroke survivors within five years, and represents a significant impediment to their quality of life (1, 5, 6). Healthcare providers and caregivers of stroke survivors have identified an understanding of cognitive changes after stroke as the foremost research priority in the field (7). Additionally, a survey of over 1200 stroke survivors found that almost 60% identify problems with concentration and memory as an unmet therapeutic need (8).

Delayed cognitive decline after stroke, or infarct-induced neurodegeneration, comprises approximately two thirds of the ten-year dementia risk, is not mitigated by preventing additional strokes, and is not associated with stroke location or severity (1, 9, 10). It is distinct from initial cognitive impairment, which is directly related to the location and severity of the infarct (11, 12). Infarct-induced neurodegeneration can be modelled in wildtype mice by inducing a stroke in the sensory cortex (13). Adult mice exhibit no acute cognitive effect from the stroke, but then develop a cognitive deficit by 7 weeks, progressive loss of long-term potentiation over 14 weeks, and chronic immune cell infiltrates in the stroke scar. Notably, in this model the cognitive decline requires B lymphocytes, and we have also found B lymphocytes in the brains of humans who die with stroke and dementia (13). Together, these findings highlight an important pathologic role for the adaptive immune response in the development of infarct-induced neurodegeneration.

Here, we tested whether blocking the VLA4/VCAM1 axis would prevent infarct-induced neurodegeneration in mice. We chose to target this axis for several reasons. It is a key signaling pathway by which immune cells, including B lymphocytes, enter tissues during inflammation. The VLA4 integrin receptor on immune cells binds to endothelial VCAM1 to initiate immune cell

trafficking across the blood-brain barrier (14, 15). Also, an anti-VLA4 antibody has been tested in humans with acute stroke and found to be safe (16, 17). Additionally, expression of VCAM1 is not only increased on endothelial cells after stroke, it is also increased in aging, where blocking antibodies improve cognition in aging mice, likely through a vasculoprotective mechanism (18). Thus, we hypothesized that blocking the VLA4/VCAM1 axis might improve cognition via both immune-dependent and vascular-dependent mechanisms in our mouse model of infarct-induced neurodegeneration. To test this, we treated middle-aged male and female mice with either anti-VCAM1 or anti-VLA4 antibodies and used Barnes maze and novel object recognition to test cognitive outcomes. In addition, we investigated underlying mechanisms using immunostaining and single-cell RNA sequencing. Our findings support a critical role for the VLA4/VCAM1 axis in the development of infarct-induced neurodegeneration and identify this axis as a potential therapeutic target to prevent cognitive decline after stroke.

Methods:

Sex as a biological variable

Our study examined male and female animals, and similar findings are reported for both sexes.

Mice

Adult (3 month old) male and middle-aged (10 month old) male and female C57BL/6J mice were purchased from Jackson Laboratory (#000664). Animals were group housed 3-5 mice per cage and allowed to acclimate for at least 1 week prior to experimentation. All experiments were performed in accordance with protocols approved by the Stanford University Institutional Animal Care and Use Committees.

Stroke surgeries

Stroke surgeries were performed as previously described (19). Briefly, mice were anesthetized with ~2% isoflurane in 100% oxygen and maintained at 37°C with a temperature-controlled heating pad for the duration of the surgery. The incision site was cleaned with chlorhexidine (Henry Schein #5680808), and an incision was made along the skull. Next, the temporalis muscle was transected so that the middle cerebral artery (MCA) was visible through the skull. A craniotomy was drilled directly above the MCA, the meninges were carefully removed, and the MCA was permanently cauterized. The muscle and skin were replaced, and the incision closed with surgi-lock glue (Meridian #78657941). Sham mice underwent the same procedure, including removal of meninges, but did not undergo MCA cauterization. Mice subsequently received a single subcutaneous dose of cefazolin (25 mg/kg; VWR #89149-888) and buprenorphine SR (1 mg/kg; Henry Schein #6030894) for infection prophylaxis and analgesia, respectively. Middle-aged (10 month old) mice were then kept in a warmed cage until they were awake and mobile, approximately 30 minutes following the surgery. Adult (3 month old) sham and stroke mice were allowed to recover for 5 min before spending 60 min in a temperature controlled 37°C chamber in 8% oxygen/92% nitrogen (dMCAO + hypoxia stroke). The purpose of the hypoxia was to increase infarct size and reduce variability between mice, although this step significantly increases mortality in older mice and was therefore not utilized (19).

Antibody Treatment

Adult (3 month old) and middle-aged (10 month old) C57BL/6J male and female mice received injections of anti-VCAM1 monoclonal antibody (α-VCAM1, BE0027, BioXCell), anti-VLA4 monoclonal antibody (α-VLA4, BE0071, BioXCell) or the appropriate isotype control antibody (α-IC, VCAM1: BE0088; VLA4: BE0090; BioXCell) at a dose of 9 mg per kg. For experiments with an acute dosing group, the first dose at 4 hours after surgery was retro-orbital,

and subsequent doses were intraperitoneal. In experiments with no acute dosing group all doses were intraperitoneal and started at 4 days after surgery. Sham-α-IC and Stroke-α-IC mice were dosed with the appropriate isotype control antibody beginning 4 hours after stroke, and then every 3 days for the duration of the experiment, using both isotype control IgG antibodies for experiments where treatment groups included both anti-VCAM1 and anti-VLA4 antibodies. Stroke-α-VCAM1 (Acute) and Stroke-α-VLA4 (Acute) mice received a single dose of their respective antibody solution at 4 hours after surgery. They then received doses of isotype control antibody once every 3 days for the duration of the experiment. Stroke-α-VCAM1 (Chronic) and Stroke-α-VLA-4 (Chronic) mice received one dose of isotype control antibody at 4 hours after stroke, and the first dose of anti-VCAM1 or anti-VLA4 antibody 4 days after stroke. They received subsequent doses of anti-VCAM1 or anti-VLA4 every 3 days for the duration of the experiment. Thus, all mice received a total of 16 injections over the course of the experimental period by an investigator blinded to treatment group. The antibody dosing strategy is depicted visually in Figure 1A.

Cognitive Behavioral Testing:

Mice were group housed, and each cage contained a random mixture of mice from each treatment group. Male and female mice were tested in separate cohorts to avoid confounding scents. The order of testing, groups and start time of testing were maintained on each day to reduce circadian variability. Prior to the initiation of the experiment, mice were subjected to three days of handling. Prior to any testing or handling on a given day, mice were acclimated to the testing room for at least 60 minutes.

Barnes Maze

A Barnes maze protocol was utilized as previously described with minor modifications for 10 month old mice (18, 20). Briefly, a circular maze containing 16 holes around the outer edge

was centered on a pedestal and elevated approximately 1 meter above the floor. All holes were open to the floor except for the escape hole, which consisted of a PVC elbow joint connector. Distinct visual cues were placed at four equally spaced points around the maze. An overhead light, two standing lights and a fan blowing on the maze provided an aversive environment, so that mice would learn the escape hole location, while also serving as supplemental visual cues. The escape hole position was aligned with one of the visual cues and remained fixed for all trials and all days. Mice performed four trials per day for four consecutive days. The starting location of the mouse was moved relative to the escape hole position at the start of every trial. Escape latency was defined as the time for a mouse to enter the escape hole. When a mouse failed to locate the escape hole within 90 seconds, it was gently guided towards the escape hole and assigned an escape latency of 90 seconds. The maze and escape holes were thoroughly cleaned with 10% EtOH after every trial and with 70% EtOH at the end of every testing day to eliminate olfactory cues. Testing was performed by an investigator blinded to experimental conditions.

Novel Object Recognition:

The novel object recognition task was performed as previously described (18, 20). Briefly, each cage of mice was habituated to an empty arena ($40 \times 40 \times 35$ cm^3) containing wall-mounted visual cues for 5 min. Mice were then individually given one 5 min trial during which they explored two identical objects in fixed positions in the middle of the arena. Animals were randomly assigned to identical starting objects and new object pairs were utilized for each testing timepoint. The testing phase began 2 hours after completion of the first exploration phase. In the testing phase, mice explored the same arena for 5 min but with one object replaced by a novel, distinct object. The arena and objects were thoroughly cleaned with 10% EtOH to eliminate residual odors between mice and between testing sessions. Object interaction was defined as sniffing or exploring within 2 cm of an object or climbing on an object (excluding time spent without movement on top of an object), and was manually timed in a blinded fashion. To assess

performance on the task, a discrimination index was calculated using the formula [(t_{novel}-$t_{familiar}$)/(t_{novel}+$t_{familiar}$)] to represent the proportion of time spent on the novel object. A score between 0 and -1 indicates a preference for the familiar object, a score between 0 and +1 indicates a preference for the novel object, and a score of 0 demonstrates no object preference.

Mouse Brain Immunohistochemistry and Immunofluorescence

Immunohistochemistry staining was performed as previously described on PFA-fixed 40 µm coronal brain sections using 3,3'-diaminobenzidine visualization (13, 21). Primary antibodies were against B220 (biotinylated, 1:500; BD Biosciences, 553085), CD3ε (1:500; BD Biosciences, 550277), and NeuN (1:500; Millipore, MAB377B). The specificity of primary antibody staining was confirmed using control sections treated with secondary antibody alone, and by visual inspection of expected cellular morphology. Images were taken using a Keyence BZ-X710 microscope. Quantification of immunostaining was performed on two consecutive sections per mouse by a researcher blinded to the treatment group. Images were taken at 20x magnification, and quantification was performed on the full field of view. B220 immunostains were quantified using thresholding in ImageJ and reported as percent of the area covered by antibody staining. The total number of CD3+ T cells per field of view was also counted using ImageJ. For atrophy quantification, every 6th section was stained using NeuN with a cresyl violet counterstain and captured with a slide scanner (PrimeHisto XE Histology # 489780). ImageJ was used to manually trace the infarct core, ipsilateral hemisphere, and contralateral hemisphere. Total brain atrophy was calculated and reported as percent loss of volume compared to the contralateral hemisphere.

Immunofluorescent staining was also performed as previously described using standard staining techniques (21). Primary antibodies were used against CD13 (1:500; Bio-Rad, MCA2183GA), CD31 (1:200; Novus Biologicals, AF3628 or 1:300, BD Biosciences, 550274), fibrinogen (1:1000; DAKO, A0080), and GFAP (1:1000; Abcam, Ab4674). To image, Z-stacks of 5 images each were taken at 40x magnification using a Leica TCS-SPE confocal microscope in

the medial peri-infarct region of the cortex, defined as one field of view away from the stroke border and at least one view field above the corpus callosum, or in the stroke core. A GFAP co-stain was used to define the stroke border and imaging location. Two brain sections per mouse were used for analysis. Sections were excluded from the analysis if they showed irregular cellular morphology. Pericyte vascular coverage was quantified in the peri-infarct cortex using ImageJ by first defining vasculature by tracing the CD31 stain and then estimating the percent of total CD31+ vessel surrounded or covered by CD13+ staining. If only one side of the vessel was closely associated with an adherent pericyte, this was counted as 50% vessel coverage. The average CD13+ vessel coverage was then calculated for each animal. Vessel number and length were calculated from the trace of the CD31 stain. Extravascular fibrinogen was quantified with a custom written macro that created a mask of the CD31 stain and then quantified the fibrinogen stain outside of the vasculature using thresholding in images from the stroke core and peri-infarct cortex.

Single Cell RNA Sequencing

Brain dissociation

Brain tissue was dissociated with the Miltenyi neural dissociation kit following the manufacturer's instructions, with minor adjustments to optimize the isolation of endothelial and immune cells. In brief, 4–5 mice per treatment group were anesthetized with ketamine/xylazine solution and perfused with 15mL ice cold phosphate buffered saline (PBS) following cardiac blood collection. The stroke core and peri-infarct cortex, defined as ~2mm surrounding the visible lesion, were dissected and pooled by condition, minced, and digested using the neural dissociation kit (Miltenyi, 130–092-628). Brain homogenates were further diluted in Dulbecco's PBS (dPBS) and filtered through a 100 µm strainer. The filtered homogenate was then centrifuged (300 *g* for 10 minutes) and the pellets were resuspended in 0.9 M sucrose in dPBS followed by centrifugation for 20 minutes at 850 *g* at 4 °C to separate the myelin. Cell pellets were resuspended in FACS

buffer (1% BSA in PBS with 2 mM EDTA) and blocked for 5 min on ice with Fc block (CD16/CD32, BD 553141), followed by staining for 10 minutes with anti-CD31-PE/TR594 (1:200, BD 563616) and anti-CD45-PE/Cy7 (1:200, BD 103114) antibodies. Dead cells were excluded by staining with SYTOX Blue Dead Cell Stain (1:5,000, Thermo Fisher Scientific S34857).

Fluorescence activated cell sorting

Brain endothelial and immune cells were sorted on the FACSAria 3.3 (BD Biosciences) system using the FACSDiva software (BD Biosciences). Cells were gated on forward scatter (FSC, size) and side scatter (SSC, internal structure). FSC-A and FSC-W plotting was used to discriminate single cells from cell doublets or aggregates. SYTOX Blue+ dead cells were also excluded via gating. CD31+CD45− cells were defined as the endothelial cell population, and CD31lowCD45+ cells were defined as the immune cell population. Cells were sorted into 0.1% BSA solution with 0.2U/μL RNAse inhibitor in PBS and then pelleted at 400 *g* for 5 minutes at 4 °C. They were then resuspended in 50 μl 0.1% BSA with 0.2U/μL RNAse inhibitor before proceeding to processing for single-cell RNA-sequencing.

RNA Extraction, Library Preparation, and RNA Sequencing

Reagents of the Chromium Single Cell 3' GEM & Gel Bead Kit v3.1 (10X Genomics, 1000121) were thawed and prepared according to the manufacturer's protocol. Cells and master mix solution were adjusted to target 10,000 cells per sample and loaded on a standard Chromium Controller (10X Genomics, 1000204) according to manufacturer protocols. We applied 11 PCR cycles to generate cDNA. Library construction was conducted using the Chromium Single Cell 3' Library Construction Kit v3 (10X Genomics, 1000121). All reaction and quality control steps were carried out according to the manufacturer's protocol and with recommended reagents, consumables, and instruments. Quality control of cDNA and libraries was conducted using a Bioanalyzer (Agilent) at the Stanford Protein and Nucleic Acid Facility. Illumina sequencing of the

resulting libraries was performed by Novogene (https://en.novogene.com/) on an Illumina NovaSeq S4 (Illumina). Base calling, demultiplexing, and generation of FastQ files were conducted by Novogene.

Data processing & Analysis

Cell Ranger (v.6.0.0) analysis pipelines were utilized to align reads to the mm10-GRCh38 hybrid reference genome and count barcodes/UMIs. Reads mapping to introns were not counted. Outliers with a high ratio of mitochondrial (more than 10%, fewer than 400 features) relative to endogenous RNAs and homotypic doublets (more than 6,000 features) were removed in Seurat. Cells were also removed if they expressed fewer than 100 unique genes. Genes not detected in any cell were removed from subsequent analysis. Log-normalized (scale factor 10,000 and pseudocount of 1) expression values of genes generated by the Seurat NormalizeData command were used for clustering and differential gene expression analysis.

Mitochondrial and cell cycle gene regression was performed to ensure that clustering reflects true cell type identities. Principal component analysis was performed on the 2000 most variable genes of the dataset followed by UMAP clustering using the Seurat R Package (v. 4.3.0.1) on the first 20 principal components.

Identification of significant clusters was performed via the standard FindClusters command in Seurat with a 1.0 resolution. CD31+ and CD45+ cells were sub-clustered based on *Pecam1* and *Ptprc* expression, respectively. CD31+ cells and CD45+ cells underwent principal component analysis and were re-clustered on a resolution parameter of 0.2 and 0.4, respectively. Cell counts were performed once the clusters were subset by condition. To pass QC, cells had a minimum of 300 reads, and on average had 5594 reads and 2208 expressed genes per cell. The annotation of each cluster was manually determined using published marker genes for each cell subtype (Supplementary Table 1). Next, MAST differential gene expression analysis between conditions was performed using Mast (v. 1.24.1), and Gene Ontology pathway analysis was

performed with Enrichr (22–24). Finally, the normalized average expression of each gene within each cluster was generated using the Dotplot function of Seurat and plotted with GraphPad Prism 9.

Plasma Proteomics:

Blood Collection and Processing into Plasma

Blood was collected from the left ventricle using an EDTA-impregnated syringe, prior to perfusion for brain collection. Whole blood was deposited into Microvette 500 K3EDTA tubes (Sarstedt #201341), and tubes were centrifuged at 4 °C for 15 minutes at 2,000*g*. The resulting supernatant was collected as plasma and stored at -80 °C prior to use for proteomic analysis by SomaLogic Operating Co., Inc (Boulder, CO). We utilized the full SomaScan platform, which yielded a total of 5,284 proteins.

Somalogic Proteomics Analysis

Individual protein differences between Stroke-α-IC or Stroke-α-VCAM1 chronic treatment groups were analyzed with a Mann Whitney test with $p < 0.05$ considered significant. Statistical outliers were removed utilizing the ROUT method (Q = 0.1%). A univariate Spearman correlation was performed to analyze the relationship between protein concentration, regardless of treatment group, and cognitive function. To assess cognitive function, a cognitive score was calculated by averaging the Barnes maze performance from trials 3 & 4 of the final day of testing for each mouse in Figure 1B. Therefore, a lower cognitive score represents better cognitive function.

Statistics:

Experimenters were blind to treatment status throughout data collection and analysis. Statistical testing was performed in GraphPad Prism 10 or R (version 4.2.2). Behavioral data were analyzed with a two-way repeated measures ANOVA with Tukey's post-hoc test. Immunostaining

data were analyzed with a Student's t test (2 groups) or one-way ANOVA with Tukey's post-hoc test (3 or more groups). Plasma proteomic data were analyzed with a Mann Whitney test. For all statistical testing, $p < 0.05$ was considered statistically significant.

Study Approval:

All experiments were performed in accordance with protocols approved by the Stanford University Institutional Animal Care and Use Committees following ARRIVE guidelines.

Data availability:

All data is available upon request from the corresponding author. Values for all data points contained in graphs are reported in the Supporting Data Values file. Single cell RNA sequencing data can be accessed through GEO (Accession # GSE300564).

Results:

Chronic anti-VCAM1 treatment prevents cognitive decline in middle-aged mice

To compare the impact of acute versus chronic blockade of the VLA4/VCAM1 axis on infarct-induced neurodegeneration, we first tested two dosing paradigms, acute or chronic using a VCAM1 blocking antibody (Figure 1). As expected for this mouse model, male and female mice that received α-IC perform normally on the Barnes maze and novel object recognition tasks before and 1 week after stroke, then exhibit delayed cognitive decline when tested 6 weeks after stroke (Figure 1B-E). In the acute paradigm, a single dose of α-VCAM1 was given at 4 h after stroke (Stroke-α-VCAM1 Acute) to block initial transit of immune cells into the brain. This acute strategy did not prevent late cognitive decline after stroke in male mice (Figure 1B,D). In contrast, male mice treated chronically with α-VCAM1 (first at 4 days, then every 3 days; Stroke-α-VCAM1 Chronic) do not develop a cognitive deficit after stroke in either task (Figure 1B, D). This was also

true when the experiment was repeated in female mice (Figure 1C, E). Thus, chronic, but not acute, treatment with α-VCAM1 prevented delayed cognitive decline after stroke.

Anti-VCAM1 treatment prevents adaptive immune cell trafficking into the brain

There was no difference in brain atrophy late after stroke in middle-aged (10 mo) male or female mice after either acute or chronic α-VCAM1 administration (Supplementary Figure 1). Thus, the protective effects of α-VCAM1 treatment are not mediated by reducing stroke size or subsequent atrophy. We next examined T and B lymphocyte infiltration into the brain to ask if this is associated with cognitive effects (Figure 1F-H). As with cognition, acute treatment had no effect on either T or B lymphocyte infiltration into the brain, while chronic α-VCAM1 treatment did reduce lymphocyte infiltration. It reduced the number of CD3+ T cells in the infarct core by 44% in male and 41% in female mice. Similarly, chronic α-VCAM1 treatment reduced the percent area covered by B lymphocytes in the stroke core by 53% in male and 62% in female mice (Figure 1H, I). Thus, reduction in adaptive immune cells but not in brain atrophy is associated with the prevention of cognitive decline after stroke with chronic α-VCAM1 treatment.

Chronic anti-VLA4 treatment prevents cognitive decline after stroke

We next asked whether blocking VLA4, the binding partner of VCAM1 on immune cells, would be beneficial and whether it would be more or less effective than targeting VCAM1. As expected, middle-aged (10 mo) male mice treated with an isotype control antibody (Stroke-α-IC) developed a robust cognitive deficit in both the Barnes maze and novel object recognition tasks at 6 weeks after stroke, compared to Sham-α-IC mice (Figure 2). This was also replicated with an independent cohort of female mice (Supplementary Figure 2). Cognitive decline was prevented equally in α-VCAM1 Chronic and α-VLA4 Chronic treatment groups on both the Barnes maze and novel object recognition tasks in both male and female mice (Figure 2, Supplementary Figure

2). Moreover, both α-VCAM1 and α-VLA4 treatment maintained the cognitive performance of mice with chronic stroke such that it was equivalent to that of sham animals at all timepoints, on both cognitive tasks, and in mice of both sexes.

Chronic anti-VLA4 treatment does not prevent adaptive immune cell trafficking

As with α-VCAM1 treated middle-aged (10 mo) mice, there was no effect on brain atrophy in adult (3 mo) mice after α-VCAM1 or α-VLA4 chronic treatment compared to stroked mice treated with isotype control antibody (Stroke-α-IC; Supplementary Figure 3). Chronic α-VCAM1 again significantly reduced T lymphocyte infiltration into the stroke core by 41% (Figure 3A) and B lymphocyte infiltration by 83% (Figure 3C). In contrast, chronic α-VLA4 did not change T or B cell trafficking into the infarct core (Figure 3B, D), despite the fact that it had equivalent effects on cognition as α-VCAM1 treatment. Similarly, and consistent with our previous findings, a single acute dose of either α-VCAM1 or α-VLA4 (Stroke-α-VCAM1 Acute or Stroke-α-VLA4 Acute, respectively) did not affect T or B lymphocyte trafficking to the infarct core (Figure 3).

Both anti-VCAM1 and anti-VLA4 treatment promote vessel growth & maturation

We next hypothesized that antibody treatment may induce transcriptional changes in immune and/or endothelial cells, that may explain why both antibody treatments were equally effective at preventing cognitive decline, despite α-VCAM1 reducing T and B lymphocyte numbers while α-VLA4 did not. We therefore performed single cell RNA sequencing of both brain immune (CD45+) and endothelial (CD31+) cells. We isolated cells from the stroke scar of mice from all four treatment groups in Figure 2. This includes stroke and sham mice treated with isotype control antibody, and stroke mice treated chronically with either α-VCAM1 or α-VLA4. We analyzed 15,263 total cells (7,942 CD45+ and 7,321 CD31+). Cells were clustered with the UMAP algorithm to reduce dimensionality, and cell-specific markers were used to annotate 11 CD45+ clusters,

comprising all major peripheral and brain-resident immune cell types (Figure 4A; Supplementary Figure 4B). Similarly, we identified 5 CD31+ cell clusters; arterial, 2 capillary and 2 venous endothelial cell populations (Figure 4B; Supplementary Figure 4A).

As a fraction of total cells counted, the proportion of peripheral immune cell clusters in the brain increased after stroke. Congruent with our histology results showing elevated lymphocyte infiltration after stroke, the proportion of T cells increased from 6.2% in Sham-α-IC to 11.2% in Stroke-α-IC, and the proportion of B cells also increased from 1.9% to 5.2% in the same groups (Supplementary Figure 4C). Chronic α-VCAM1 or α-VLA4 treatment then normalized proportions of T and B lymphocytes down to that of the the Sham-α-IC group. In chronic α-VCAM1 treated stroke mice (Stroke-α-VCAM1 Chronic), the proportion of T cells was 5.1% and B cells 1.4% (Supplementary Figure 4C). In chronic α-VLA4 treated stroke mice (Stroke-α-VLA4 Chronic), the proportions were 7.4% and 1.7%, respectively. Unexpectedly, after stroke there was a higher proportion of cells within the two capillary clusters, and fewer cells in the arterial cell cluster. Specifically, stroke increased the proportion of capillary endothelial cells from 32.5% in Sham-α-IC to 42.3% in Stroke-α-IC and reduced the proportion of arterial endothelial cells from 62.2% in Sham-α-IC to 53.5% in the Stroke-α-IC sample. Both α-VCAM1 and α-VLA4 chronic treatment also slightly increased the proportion of capillary endothelial cells and reduced the proportion of arterial endothelial cells after stroke (Supplementary Figure 4D).

Despite the increase in proportion of peripheral immune cells in the stroke brain at this chronic timepoint, there were very few significant ($p<0.05$; $Log_2FoldChange>|0.5|$) transcriptomic changes in these cells, compared to cells from the Sham-α-IC sample (Supplementary Figure 5). A similar pattern was observed after α-VCAM1 or α-VLA4 treatment, compared to the Stroke-α-IC group. In fact, other than the Monocyte-1 cluster (Figure 4A, bottom cluster) which had 94 differentially expressed genes when comparing Stroke-α-VLA4 to Stroke-α-IC, no other

bioinformatic comparison within peripheral immune cell types found more than 19 differentially expressed genes.

In contrast, we found dramatic changes in gene expression in endothelial cells with stroke alone (Sham-α-IC vs. Stroke-α-IC), and with Stroke-α-VCAM1 or Stroke-α-VLA4 treatment compared to Stroke-α-IC. When using a differentially expressed gene (DEG) cutoff of $p<0.05$ and $Log_2FoldChange>|0.5|$ within each subpopulation of endothelial cells, arterial cells were the most changed by stroke, with increased expression of 501 genes and decreased expression of 473 genes (Figure 4C). Additionally, chronic treatment with α-VCAM1 or α-VLA4 primarily affected the arterial and capillary-1 (left cluster, Figure 4B) endothelial cell clusters, which were also the two clusters with the largest proportional population changes after stroke, or either antibody treatment. After α-VCAM1 treatment, arterial endothelial cells increased expression of 200 genes and decreased expression of 70 genes, while capillary-1 endothelial cells increased expression of 50 and decreased expression of 28 genes, compared to Stroke-α-IC cells. Similarly, after chronic α-VLA4 treatment, arterial cells increased expression of 268 genes and decreased expression of 237 genes, while capillary-1 cells increased expression of 120 and decreased expression of 86 genes. In contrast to the large number of gene expression changes when comparing antibody treatment to the Stroke-α-IC group, the differences between the α-VCAM1 and α-VLA4 treated groups were minimal. Specifically, there were <10 differentially expressed genes when directly comparing α-VCAM1 to α-VLA4 treated endothelial cells from any cluster (Figure 4C).

We next used over-representation analysis to understand the biological pathways underpinning the transcriptomic changes induced by stroke, and by chronic α-VCAM1 or α-VLA4 antibody treatment after stroke. We focused on the arterial and capillary-1 clusters because they had the highest number of changed genes. In the arterial cell cluster, stroke reduced expression of genes in pathways involving cell proliferation and development and new vessel growth. In

contrast, both α-VCAM1 and α-VLA4 treatment enriched multiple pathways related to cell proliferation and migration, pointing to angiogenesis and new vessel growth after chronic antibody treatment (Figure 4D,E, blue arrows). Both antibody treatments also enriched multiple pathways involved in vessel maturation compared to the Stroke-α-IC group in the arterial cell cluster (Figure 4D,E, red arrows). Consistent with abnormalities in vascular growth and maturation in chronic stroke, many of the same genes involved in cellular proliferation pathways were also reduced in the capillary-1 cluster in the Stroke-α-IC group compared to Sham-α-IC. After both chronic α-VCAM1 and α-VLA4 treatment, many of the same pathways were enriched in the capillary-1 cluster, compared to the Stroke-α-IC condition (Figure 4F, G).

Indeed, key genes involved in cell-cell junction formation, pericyte recruitment and cytoskeleton assembly, all of which are critical for vessel growth and maturation, all followed a consistent pattern. Overall, stroke reduced expression of genes related to vascular growth and maturation and reduced the proportion of endothelial cells expressing the genes (left panel, Figure 5A). In contrast, chronic treatment of stroked mice with either VCAM1 or VLA4 blocking antibodies reversed this effect, and we found increased expression per cell (blue color, Figure 5A) and/or more cells expressing each of these genes (filled circles, Figure 5A). We further investigated whether expression of selected genes was restored to sham levels by looking at the normalized average gene expression in the capillary-1 cluster, which had the most dramatic changes related to expression of genes involved in vessel maturation and the maintenance of the blood-brain barrier. Of the genes identified in Figure 5A, expression of 10 of 15 were restored to Sham-α-IC levels after chronic treatment with α-VLA4, and 8 of 15 were restored after chronic treatment with α-VCAM1. The remaining 5-7 genes were restored to ~60% of their expression relative to levels in the Sham-α-IC cells after chronic antibody treatment. Notably, gene expression of *Ctnnb1* (Catenin B), a protein within adherens junctions, followed this pattern (Figure 5B). Cell-cell junctions are critical for communication between cells of the neurovascular unit and establishment

of an intact blood-brain barrier, so we next investigated individual genes involved in pericyte recruitment, including growth factors and others that modulate the basement membrane and extracellular matrix. Expression of the growth factor *Edn3* (Endothelin 3; Figure 5C) and the collagenase *Plod2* (Procollagen Lysyl Hydroxylase 2; Figure 5D) were both reduced by stroke and restored to sham levels after α-VCAM1 or α-VLA4 chronic treatment.

Next, we performed proteomics on plasma isolated from the Stroke-α-IC and Stroke-α-VCAM1 (Chronic) groups, utilizing the full SomaLogic Proteomics Panel (5,284 total aptamers that measure plasma proteins in mice). Chronic α-VCAM1 treatment also exhibited a vasculoprotective signature. Consistent with the transcriptomic data, we observed elevated plasma protein expression of Catenin B (CTNNB1; Figure 5E), Endothelin-3 (EDN3; Figure 5F), and Procollagen Lysyl Hydroxylase 2 (PLOD2; Figure 5G). We next utilized a $p < 0.05$ cutoff to identify all proteins significantly changed after chronic α-VCAM1 treatment. We observed moderate changes in additional proteins involved in vascular growth and maintenance. These include increases with chronic α-VCAM1 treatment in Thrombin, Prolyl-4 Hydroxylase Alpha-2, Tenascin-X, Leucine-rich Repeat-containing G Protein-coupled Receptor 5, Transmembrane Serine Protease 6, and GSK3B-interacting Protein, which are all involved in vascular growth and maintenance. Conversely, the concentration of proteins associated with blood-brain barrier dysfunction such as Collagen 8A1, SARP1, Endothelin-converting Enzyme-1, Collagen 11A2, and Matrix Metalloproteinase-16 decreased after chronic α-VCAM1 treatment (Supplementary Table 2). Additionally, proteins that are downstream of the VCAM1/VLA4 signaling axis that function to open the blood-brain barrier, such as Spastin and Rho Guanine Nucleotide Exchange Factor 2, were also decreased by chronic α-VCAM1 treatment.

Given the strong biological signature of vessel growth and maturation observed with both single cell RNA sequencing and plasma proteomics, we next used immunostaining to formally quantify these processes (Figure 6). We first analyzed the number and length of CD31+ blood

vessels in the peri-infarct cortex to assess vessel growth. There was no difference in total vessel number (Supplementary Figure 6), but α-VCAM1 treated mice demonstrated a trend towards longer vessels (Figure 6A) and chronic α-VLA4 treated mice had longer vessels than isotype control antibody treated mice after stroke (Figure 6D). We next analyzed vascular pericyte coverage as a measure of blood vessel maturation and blood-brain barrier structural integrity. Both chronic α-VCAM1 and α-VLA4 treatment increase CD13+ pericyte coverage of CD31+ blood vessels by 73% and 68%, respectively, in the peri-infarct cortex (Figure 6B-C,E-F). In the contralateral cortex, there was a trend towards increased coverage in α-VCAM1 treated mice (Figure 6C), while chronic α-VLA4 increased pericyte coverage by 68% (Figure 6F). Finally, due to the critical role of pericytes in both forming and maintaining an intact blood-brain barrier, we analyzed extravascular fibrinogen leakage into the brain parenchyma. Chronic α-VCAM1 treatment completely eliminated extravascular fibrinogen leakage in the peri-infarct cortex, and there was also a strong trend towards reduced leakage in the stroke scar (Figure 7A, B). Similarly, chronic α-VLA4 significantly reduced extravascular fibrinogen leakage in both the stroke scar and peri-infarct cortex compared to Stroke-α-IC mice (Figure 7C,D). Thus, chronic treatment with α-VCAM1 and α-VLA4 increased cerebrovascular structural and functional integrity in chronic stroke.

Discussion:

We report here that during the weeks after stroke, the VLA4/VCAM1 interaction is critical for the development of infarct-induced neurodegeneration in mice of both sexes. We utilized two different antibodies to block this pathway, one against VCAM1 and one against VLA4, and demonstrated that chronic blockade robustly prevents infarct-induced neurodegeneration in both male and female mice. We observed this result in 3 experiments with anti-VCAM1 antibodies, twice in males and once in females. We then confirmed the protective effects of blocking this axis

with an anti-VLA4 antibody in two additional experiments in males and one in females. In addition, we utilized two distinct cognitive tasks to interrogate memory (novel object recognition) and learning/executive function (Barnes maze) and observed improved cognitive function in each experiment. We also demonstrated here that chronic anti-VCAM1 treatment significantly reduced B and T lymphocyte infiltration into the brain, while anti-VLA4 was not effective at reducing lymphocyte numbers. Using high-depth single cell RNA sequencing of endothelial cells, we also demonstrated that in chronic stroke there is reduced expression of genes associated with angiogenesis and vessel maturation, and that this reflects structural and functional changes in cerebrovasculature adjacent to the infarct. In contrast to their differential effects on lymphocytic infiltration, both chronic antibody treatments ameliorated these chronic stroke-induced gene expression changes, pointing to preservation of normal cerebrovasculature as a primary mechanism of action. Plasma proteomics from mice treated with chronic anti-VCAM1 compared to isotype control antibody also supports a vasculoprotective mechanism. And finally, chronic treatment with either antibody improves vascular pericyte coverage and ameliorates blood-brain barrier leakiness.

Taken together with our prior work demonstrating that B lymphocytes are critical for initiation of infarct-induced neurodegeneration (13), we hypothesize that in infarct-induced neurodegeneration there is a chronic inflammatory process where B and T lymphocytes are activated and traffic to the brain in the weeks after stroke. This leads to chronic neuroinflammation and a disrupted blood-brain barrier that remains leaky to pathological molecules such as fibrinogen. Chronic immune cell trafficking into the brain exacerbates blood-brain barrier leakiness, resulting in a positive feedback loop which propagates chronic inflammation and blood-brain barrier dysfunction. Over time, this leads to cognitive decline (Figure 8). When we block the VLA4/VCAM1 axis via chronic but not acute treatment with anti-VCAM1 or anti-VLA4, it interrupts the positive feedback loop by promoting generation of mature blood vessels with intact tight junctions, recruiting pericytes and preventing chronic immune cell influx with a mature and intact

blood-brain barrier (Figure 8). Notably, the effects of anti-VCAM1 are more pronounced than those of anti-VLA4 on lymphocyte infiltration, strongly supporting the hypothesis that vascular integrity is the primary mechanism by which chronic anti-VCAM1 and anti-VLA4 treatment preserve cognitive function. The effects on vasculature are more robust and consistent between both antibody treatments compared to the effects on immune cell infiltration, and a vasculoprotective mechanism is reflected in not only transcriptomics but also in our plasma proteomic and immunostaining data. Thus, it is likely that the effects of an activated VLA4/VCAM1 axis on cerebrovascular function are most important in eroding cognitive function, and conversely, that blocking VLA4 or VCAM1 preserves cognition due to maturation of vasculature and preservation of its function, including maintenance of the blood-brain barrier.

This work represents the first time that VCAM1 and VLA4 have been blocked chronically after stroke, however there is precedent that blockade of this signaling pathway might affect both immune cell infiltration and blood-brain barrier integrity. In rodent models of stroke, acute dosing of anti-VLA4 robustly reduces leukocyte infiltration into the brain, and also reduces infarct size in some but not all studies (25–29). In rodent models of the autoimmune disease multiple sclerosis, experimental autoimmune encephalitis, anti-VLA4 treatment reduces B and T lymphocyte trafficking into the brain, demyelinating lesion size and axonal loss (30–33). Additionally, while there is minimal leukocyte trafficking to the brain during normal aging, chronic anti-VCAM1 treatment of aged mice reduces neuroinflammation and endothelial cell activation, and restores cognitive function (18). Our study highlights an important role for the VLA4/VCAM1 axis in vascular permeability, likely related to its critical role in leukocyte diapedesis. Indeed, the VCAM1/VLA4 axis has a direct effect on vascular permeability in cancer models, where activating this axis induces hyperpermeability of an endothelial monolayer *in vitro* (34, 35). This increased permeability is likely related to structural rearrangement of tight and adherens junctions, as well as cytoskeletal reassembly, mediated via multiple genes including *Ctnnb1*, *Rhoc* and *Magi1* which are downstream of VCAM1 signaling in endothelial cells (36).

To investigate the roles of immune and vascular mechanisms of action in infarct-induced neurodegeneration, we performed single cell RNA sequencing on both immune cells and endothelial cells. Despite significant work analyzing immune cell populations in acute stroke, little is known about gene expression changes in the chronic phase. We are the first, to our knowledge, to interrogate the transcriptome of immune cells months after stroke. Despite significant pro-inflammatory activation of immune cells acutely (37, 38), we observed very few gene changes in chronic stroke. While it is possible that subtle gene expression changes may be masked due to processing artifacts during tissue digestion, we did observe a robust increase in the proportion of peripheral immune cells in the brain after stroke (39). Specifically, we observe high numbers of B and T lymphocytes in the brain after stroke, which were significantly reduced after anti-VCAM1 treatment. This reduction in B and T lymphocytes was also associated with improved cognition in our study. This is consistent with our previous study in adult mice where we showed that ablating B cells beginning 5 days after stroke prevents delayed cognitive decline (13). In addition, humans who die with infarcts and dementia have increased numbers of B cells in and around the stroke, and higher MBP antibody titers are associated with worse cognitive trajectories in stroke survivors (13, 40, 41).

In the context of this robust literature implicating B lymphocytes in infarct-induced neurodegeneration, it was unexpected and intriguing that anti-VLA4 treatment had a strong positive effect on cognition without meaningfully reducing B lymphocyte numbers in the brain. Notably, in our prior human autopsy data, although overall B cell numbers were high around the infarct in people who died with infarcts and dementia, they were not high in everyone in that group. Thus, while B cells and/or autoimmune responses may be relevant for some, they may not be required in the brain for perpetuation of infarct-induced neurodegeneration in all people with post-stroke dementia. And in this mouse model of infarct-induced neurodegeneration defects in vasculature are likely more important than immune cell infiltration.

In support of a role for cerebrovascular defects in infarct-induced neurodegeneration, we saw dramatic stroke-induced changes in gene expression in endothelial cells 10 weeks after stroke. High depth sequencing allowed a high-resolution look at how different vessel segments respond to stroke. We found that endothelial cells from the arterial segment exhibited the most changes in total gene expression between sham and stroke mice, while venous endothelial cells changed the least. This is consistent with another single cell RNA sequencing study investigating how endothelial cells respond to age or acute LPS injection (42), where venous cells respond less than other vessel segments. However, in that study, capillary rather than arterial endothelial cells exhibited the most transcriptional change. This difference may reflect arterialization of new vessels that grow in the recovery phase after stroke. This has been observed after ligation of the middle cerebral artery in rats, where both the diameter and lengths of collaterals on the brain surface significantly increase one month later (43).

Overall, the stroke-induced gene expression changes we observed in both arterial and capillary endothelial cells were consistent with a loss of blood-brain barrier integrity in chronic stroke. Indeed, while immune cell transcriptional changes had largely resolved, endothelial cells retained a signal of chronic dysfunction. We observed a reduction in expression of genes involved in tight junction formation and pericyte recruitment and retention, and increased expression of genes related to blood-brain barrier permeability such as collagenases and matrix metalloproteinases. Venous endothelial cells also exhibited evidence of increased permeability, but rather than overt changes in gene expression among the population, the population of venous endothelial cells expressing endothelial permeability genes such as *Ctnnb1* and *Magi1* changed. The percent of venous endothelial cells expressing proliferation and stress response genes also increased, perhaps reflecting generally more porous and activated venous endothelium. Thus, the sequencing depth allowed us to see differential responses in the different vessel segments, however there was overall a loss of vascular integrity and increased proliferation and stress response throughout the vascular bed.

Chronic blockade of the VLA4/VCAM1 axis had an overall protective effect on cerebral vascular endothelial cells. Both antibodies reversed many of the stroke-induced gene expression changes related to blood-brain barrier dysfunction, and we also observed a modest signature in the plasma consistent with these gene changes. In both arterial and capillary endothelial cells, anti-VCAM1 and anti-VLA4 chronic treatment restored expression of genes related to tight junction formation, pericyte recruitment and pericyte retention back to sham levels. Additionally, immunostaining confirmed that either antibody was sufficient to increase pericyte coverage of endothelial cells and to block fibrinogen leakage into the brain. Thus, blockade of the VLA4/VCAM1 axis with antibody therapeutics restores blood-brain barrier integrity.

Our findings that decreased pericyte coverage and fibrinogen leakage across the blood-brain barrier in chronic stroke are detrimental in infarct-induced neurodegeneration are consistent with other neurodegenerative diseases. Chronic blood-brain barrier leakage is associated with cognitive decline in both aging and Alzheimer's disease (44–46). Moreover, chronic blood-brain barrier leakage itself can directly contribute to cognitive decline via fibrinogen, which contributes to neuroinflammation and cognitive decline in rodent models of brain injury, Alzheimer's disease, and multiple sclerosis (47–50). This may be mediated via increased synapse elimination or neuronal senescence resulting in cognitive dysfunction, which has been causally linked to neuroinflammation and blood-brain barrier breakdown after stroke (51–53). Although it is well known that there is acute pericyte loss in the infarct core after stroke (54, 55), as well as acute blood-brain barrier leakiness (56–58), little is known about vascular integrity in the chronic phase. Notably, pericyte vascular coverage is reduced in rodent models of aging, in addition to deficient pericyte remodelling after injury (59, 60). Aging is also a major risk factor for both stroke and dementia, suggesting that impaired vascular integrity with age may be an underlying causal mechanism. New work in our laboratory also demonstrates a prominent loss of pericytes in infarct-induced neurodegeneration in people, with a median value of zero pericytes associated with infarct-adjacent vessels in people who died with infarcts and dementia, but not those who died

with infarcts and no dementia (unpublished). We show here that this also happens in the mouse model, and excitingly that chronic anti-VCAM1 and anti-VLA4 treatment reduce this leakage and prevent cognitive decline in chronic stroke. Together, this evidence supports the VLA4/VCAM1 axis as a strong translational therapeutic target to improve vascular integrity.

Anti-VLA4 antibody therapy with Natalizumab is already FDA approved and used routinely in patients with multiple sclerosis where it prevents blood-brain barrier leakiness and promotes better outcomes (61–63). Indeed, there is some evidence that Natalizumab improves cognitive outcomes in multiple sclerosis (64, 65). In acute stroke, it is proven safe but had no impact on infarct size or 90 day cognitive outcomes (16, 17). However, in these clinical trials (ACTION I and ACTION II), a single acute dose of Natalizumab was given between 9 and 24 hours after stroke. Here, when we used a single dose in mice at 4 hours after stroke, this also did not improve cognition. However, when we treat mice chronically, beginning on day 4, we see robust prevention of infarct-induced neurodegeneration. Thus, chronic therapy regimens, similar to those in multiple sclerosis, may be necessary to prevent cognitive decline after stroke.

In conclusion, we report that blocking the VLA4/VCAM1 axis with chronic antibody treatment prevents cognitive decline in a middle-aged mouse model of infarct-induced neurodegeneration. We used three separate approaches–single cell RNA sequencing, plasma proteomics, and immunostaining–to demonstrate that both anti-VCAM1 and anti-VLA4 promote cerebrovascular health in chronic stroke. They both increase structural integrity of cerebrovasculature chronically after stroke, specifically inducing increased vascular coverage by pericytes and restoration of the blood-brain barrier. Future work is needed to further test these strategies to restore pericyte coverage and restore the blood-brain barrier in chronic stroke in humans to determine whether these mechanisms will benefit patients with infarct-induced neurodegeneration.

Author Contributions:

KAZ designed and performed experiments, collected and analyzed data, and wrote and edited the manuscript with comments from all authors. KB, LZ, OH, and AF performed experiments and collected data. TP, HY, DL, and TWC designed experiments. EM and NA analyzed data. MSB designed experiments and wrote and edited the manuscript.

Acknowledgments:

This work was supported by a Knight Initiative for Brain Resilience Catalyst Award (MSB), the American Heart Association/Allen Frontiers Group Brain Health Award (MSB & TWC), Alzheimer's Association Research Fellowship (KAZ), and a Leducq Transatlantic Network of Excellence award (MSB).

Figures

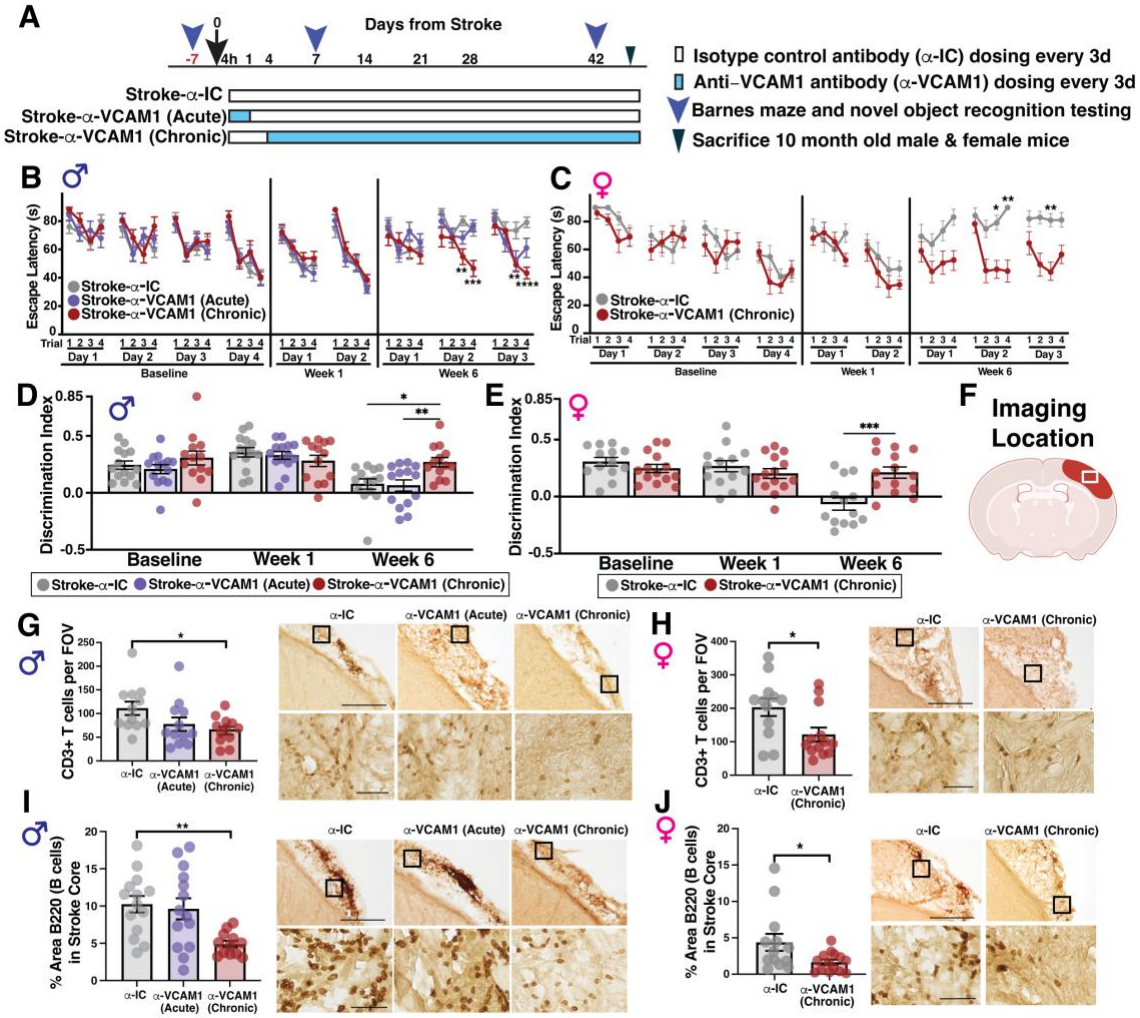

Figure 1. Chronic anti-VCAM1 antibody treatment prevents cognitive decline and reduces lymphocyte trafficking in male and female middle-aged mice. A) Diagram depicting the study design. All animals received doses at 4 hours and then every 3 days with isotype control antibody (α-IC) or VCAM1-blocking antibody (α-VCAM1) as depicted. B) Escape latency on the Barnes maze and C) discrimination index on the novel object recognition task for 10 month old male mice treated with the appropriate isotype control antibody throughout (α-IC; n=14), a single anti-VCAM1 dose at 4 hours (Stroke-α-VCAM1 Acute; n=14) or anti-VCAM1 throughout (Stroke-α-VCAM1 Chronic; n=13). D) Escape latency on the Barnes maze and E) discrimination index on the novel object recognition task for 10 month old female mice. Stroke-α-IC, n=13; Stroke-α-VCAM1 Chronic, n=14. F-J) Immunostaining for lymphocytes in the same mice at 8 weeks after stroke. F) CD3+ T cell number per field of view (FOV) into the stroke core in male and G) female mice. H) Percent area covered by B220+ (B cell) immunostaining in the stroke core of male and I) female mice, 8 weeks after stroke. Statistics, 2-way repeated measures ANOVA with Bonferroni's post-hoc test (B-C), one-way ANOVA with Tukey's post hoc test (D-E, G, I), or two-tailed Student's *t* test (H, J); Scale bar, 300 μM (top row) or 50 μM (bottom row); Error bars, mean ± SEM; *p < 0.05; **p < 0.01; ***p < 0.001; ****p < 0.0001.

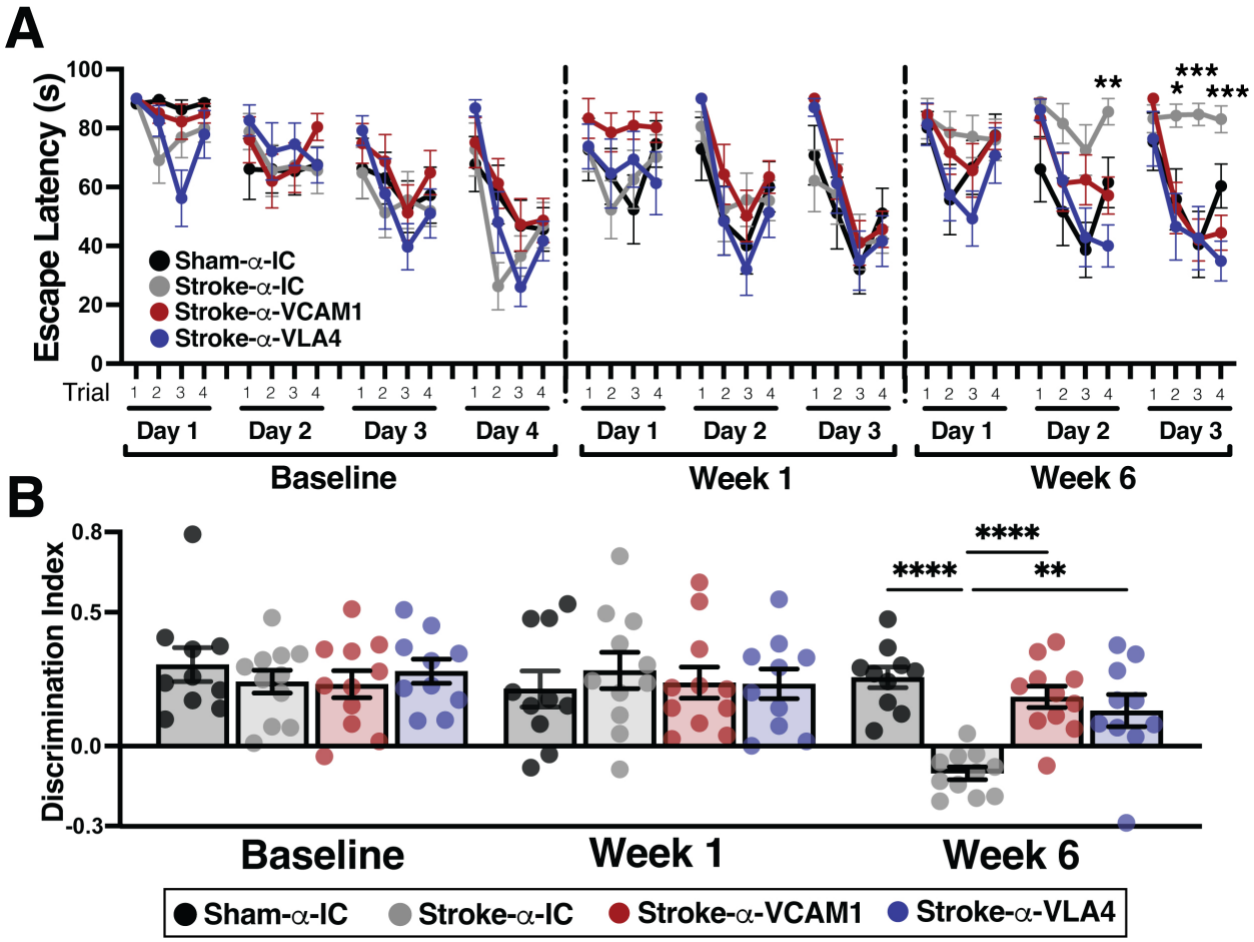

Figure 2. Both anti-VCAM1 and anti-VLA4 chronic antibody treatment prevent cognitive decline in middle-aged mice. A) Escape latency on the Barnes maze and B) discrimination index on the novel object recognition task for 10 month old male mice treated with isotype control antibody (α-IC; n=10 sham and 11 stroke), anti-VCAM1 (α-VCAM1; n=11) or anti-VLA4 (α-VLA4; n=10) chronically. Statistics, 2-way repeated measures ANOVA with Bonferroni's post-hoc test; Error bars, mean ± SEM; *$p < 0.05$; **$p < 0.01$; ***$p < 0.001$; ****$p < 0.0001$.

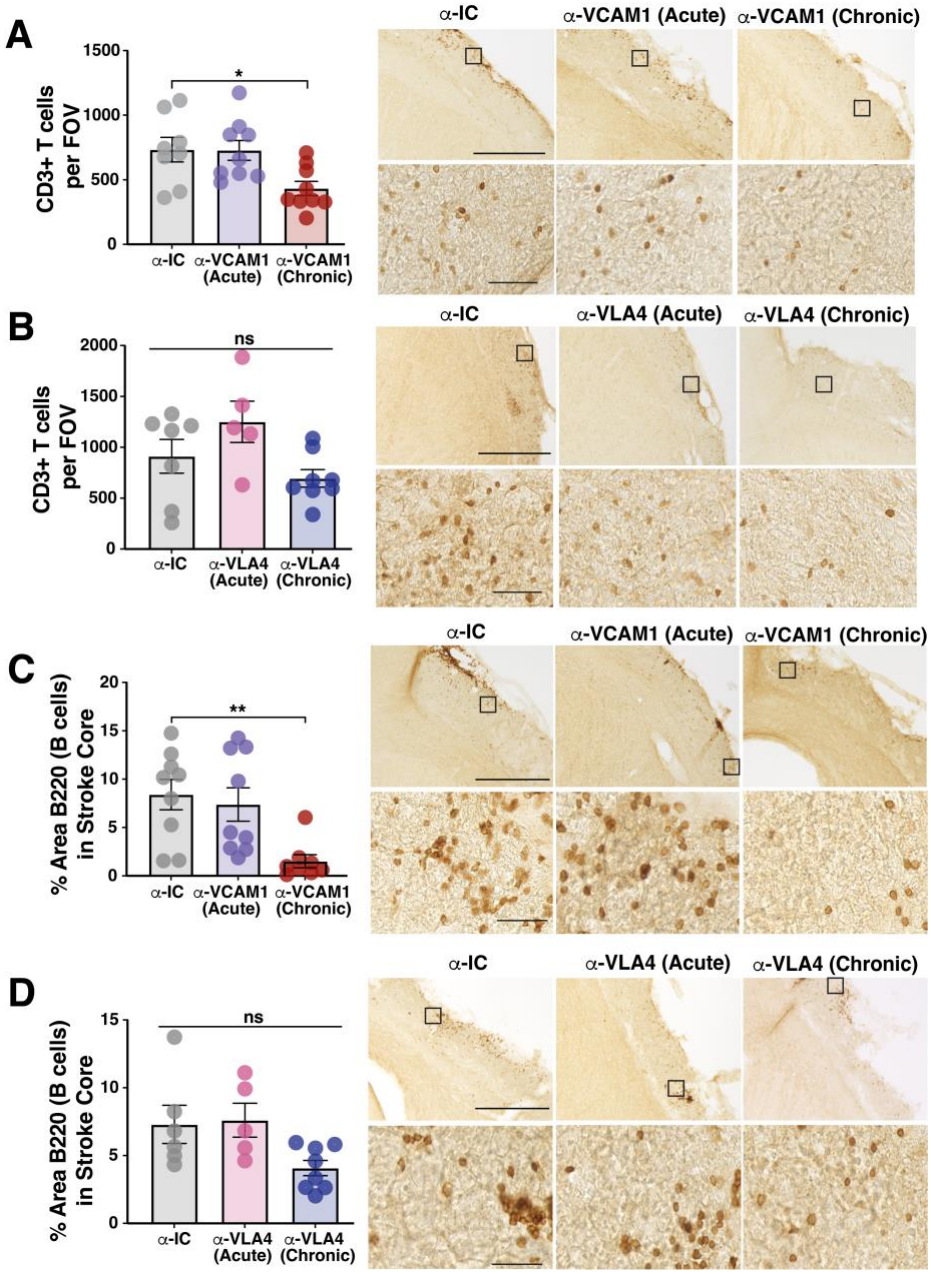

Figure 3. Chronic anti-VCAM1 is more effective at reducing lymphocyte trafficking than chronic anti-VLA4 treatment. A) Quantification and representative bright field images of CD3+ T cells in the stroke core after isotype control (α-IC, n=8), anti-VCAM1 acute (Stroke-α-VCAM1 Acute, n=9) or chronic (Stroke-α-VCAM1 Chronic, n=9) treatment, or B) isotype control (α-IC, n=7), anti-VLA4 acute (Stroke-α-VLA4, n=5) or chronic (Stroke-α-VLA4 Chronic, n=8) antibody treatment 3 weeks after stroke. C-D) Quantification and representative bright field images of B220+ B cells in the stroke core after in the same mice. Scale bar, 300 μM (top row) or 50 μM (bottom row); statistics, 2-way ANOVA with Tukey's post hoc test for group comparisons; Error bars, mean ± SEM; *$p < 0.05$; **$p < 0.01$; ***$p < 0.001$; ****$p < 0.0001$.

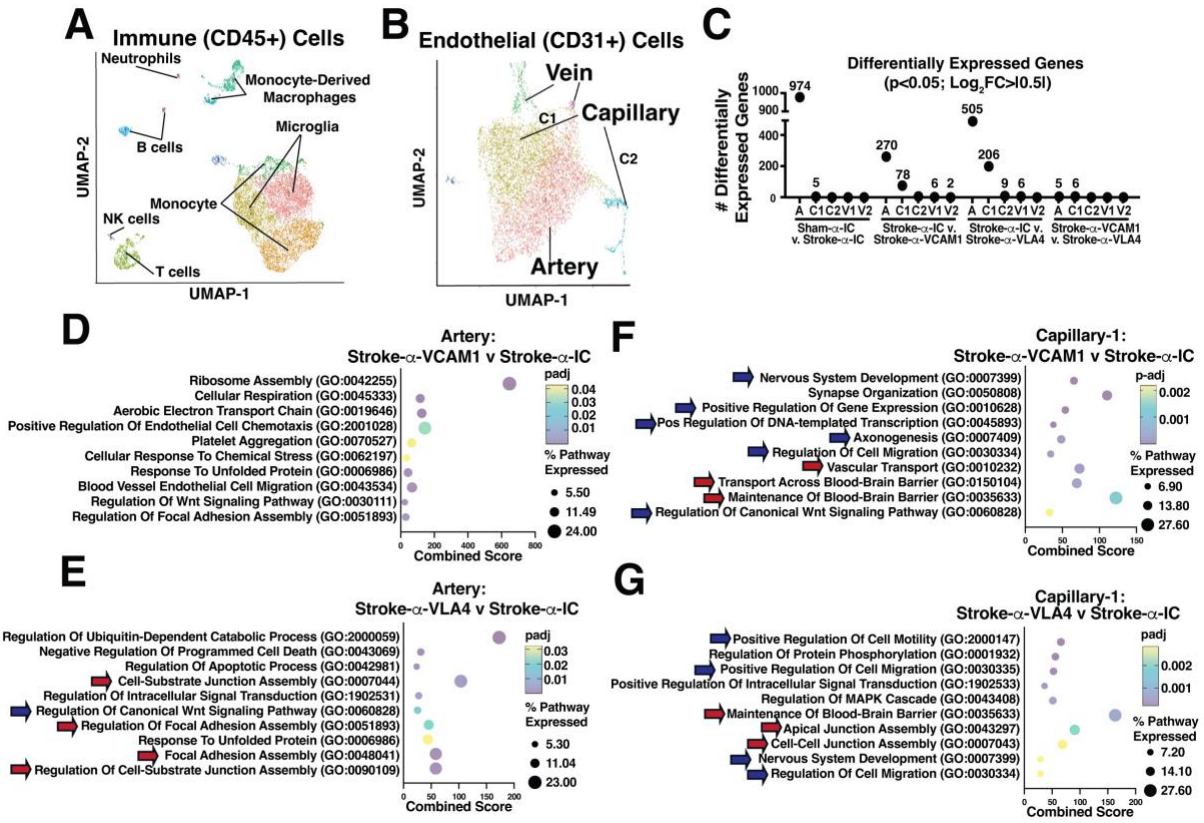

Figure 4. Anti-VCAM1 and anti-VLA4 treatment induces changes in endothelial cells which reflect generation of new and more mature blood vessels. Unbiased UMAP visualization of (A) immune and (B) endothelial cell populations isolated from the stroke scar of 10 month old male mice, 10 weeks after stroke, based on single cell RNA sequencing. Each sample represents a pool of 4-5 mice in four groups, sham and stroke mice treated with isotype control antibody (Sham-α-IC and Stroke-α-IC), and stroke mice treated chronically with anti-VCAM1 (Stroke-α-VCAM1) or anti-VLA4 (Stroke-α-VLA4) antibody. For all groups, treatment was every 3 days, beginning 4 days after surgery for a total of 10 weeks. C) A graphical representation of the number of differentially expressed genes in each subpopulation of endothelial cells, separated by the specific comparisons of interest. D-G) Over-representation pathway analysis on the differentially expressed genes in the artery and capillary-1 clusters. Comparisons are between Stroke-IgG and either Stroke-VCAM1 (D,F) or Stroke-VLA4 (E,G) treatment groups. The top pathways are included here, along with the combined score (x-axis), the percent of genes expressed within each pathway (dot size) and p value of pathway enrichment (dot color). Blue arrows identify pathways involved in vessel growth, while red arrows identify pathways involved in vessel maturation and blood brain barrier maintenance.

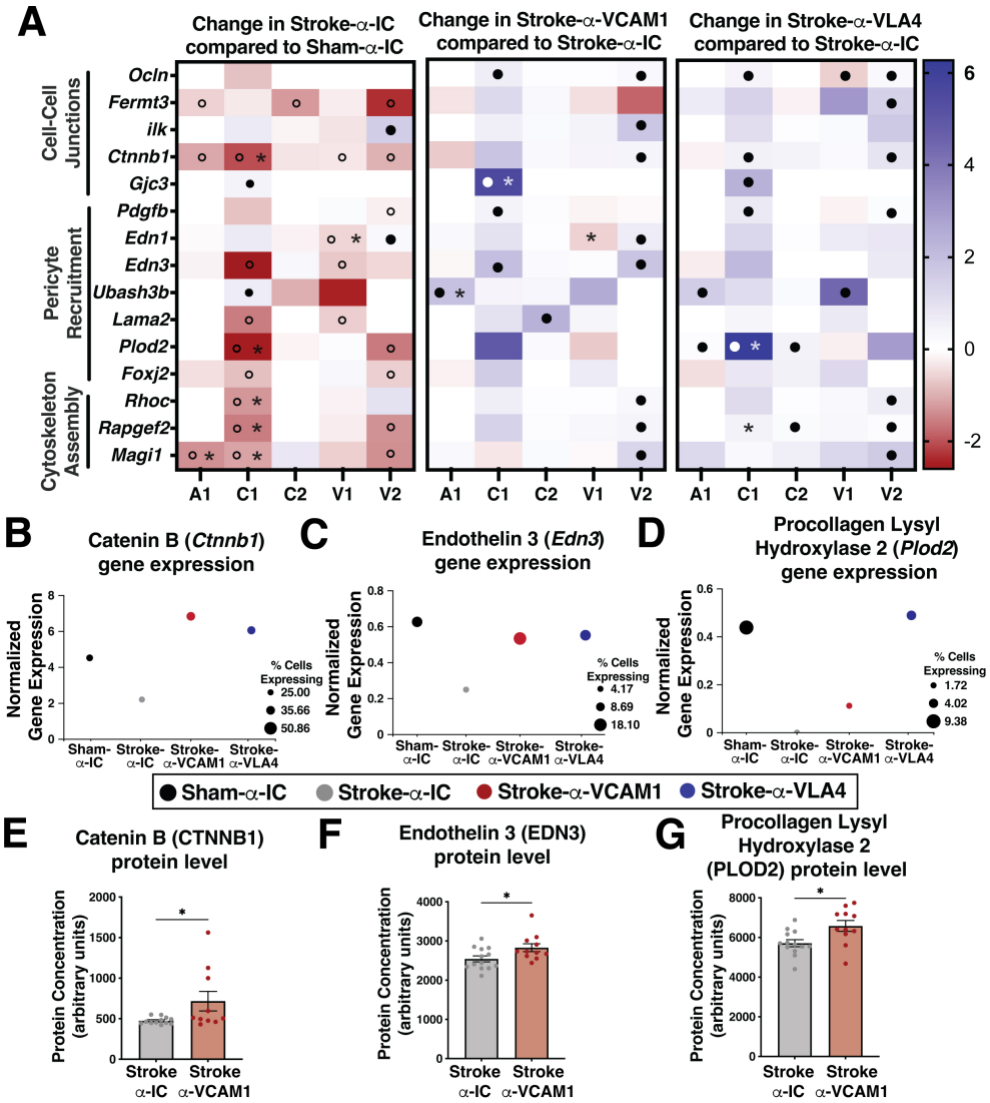

Figure 5. Genes involved in cell-cell junction formation, pericyte recruitment and cytoskeleton assembly are stimulated after anti-VCAM1 and anti-VLA4 treatment. A) Heat map comparing the Log_2Fold Change of selected genes involved in cell-cell junction formation, pericyte recruitment or cytoskeleton from each endothelial cell cluster. Three different bioinformatic comparisons are depicted from left to right: Stroke-α-IC v. Sham-α-IC; Stroke-α-VCAM1 v. Stroke-α-IC; Stroke-α-VLA4 v Stroke-α-IC. A: Artery cell cluster; C1: Capillary-1 cluster; C2: Capillary-2 cluster; V1: Vein-1 cluster; V2: Vein-2 cluster. A star represents a significant Log_2Fold Change (univariate $p < 0.05$), and a circle represents a change >10% of cells expressing the selected gene. Open circles represent decrease in the percent of cells expressing that gene, while filled circles represent an increase. B-D) Normalized gene expression (scaled transcript counts and percent of population expressing) of selected genes involved in cell-cell junction formation (B; *Ctnnb1*), pericyte recruitment (C; *Edn3*) and blood-brain barrier maintenance (D; *Plod2*) in the capillary-1 cell cluster, and how this changes with treatment. Dot size represents the % of cells within each clustering expressing the individual gene. E-G) Protein concentration from SomaLogic proteomics of Catenin B (E), Endothelin 3 (F), and Procollagen Lysyl Hydroxylase 2 (G). *$p < 0.05$, Mann-Whitney U test.

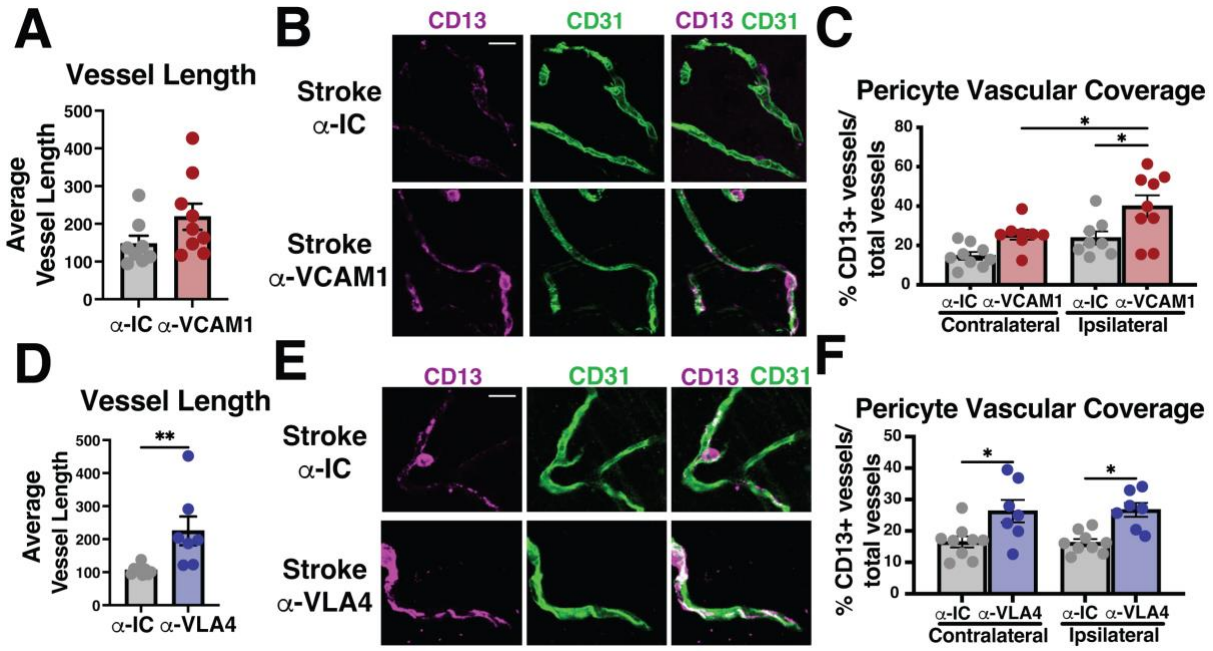

Figure 6. Effects of anti-VCAM1 and anti-VLA4 chronic treatment on vascular length and coverage by pericytes. A) Total vessel length in the peri-infarct cortex after 3 weeks of chronic isotype control (Stroke-α-IC) or anti-VCAM1 (Stroke-α-VCAM1) antibody treatment, using endothelial staining for CD31 to define vasculature. B) Representative confocal images and (C) quantification of pericyte (CD13+) coverage of CD31+ vasculature in the peri-infarct cortex or contralateral cortical region of stroked mice treated with isotype control (Stroke-α-IC) or anti-VCAM1 (Stroke-α-VCAM1) antibody. D) Total vessel length in the peri-infarct cortex after 3 weeks of chronic isotype control (Stroke-α-IC) or anti-VLA4 (Stroke-α-VLA4) antibody treatment. E) Representative confocal images and (F) quantification of pericyte (CD13+) coverage of CD31+ vasculature in the peri-infarct cortex or contralateral cortical region of stroked mice treated with isotype control (Stroke-α-IC) or anti-VLA4 (Stroke-α-VLA4) antibody. Scale bar, 20 μM; Statistics, Student's *t* test or 2-way ANOVA with Tukey's post hoc test for group comparisons; Error bars, mean ± SEM; *$p < 0.05$; **$p < 0.01$.

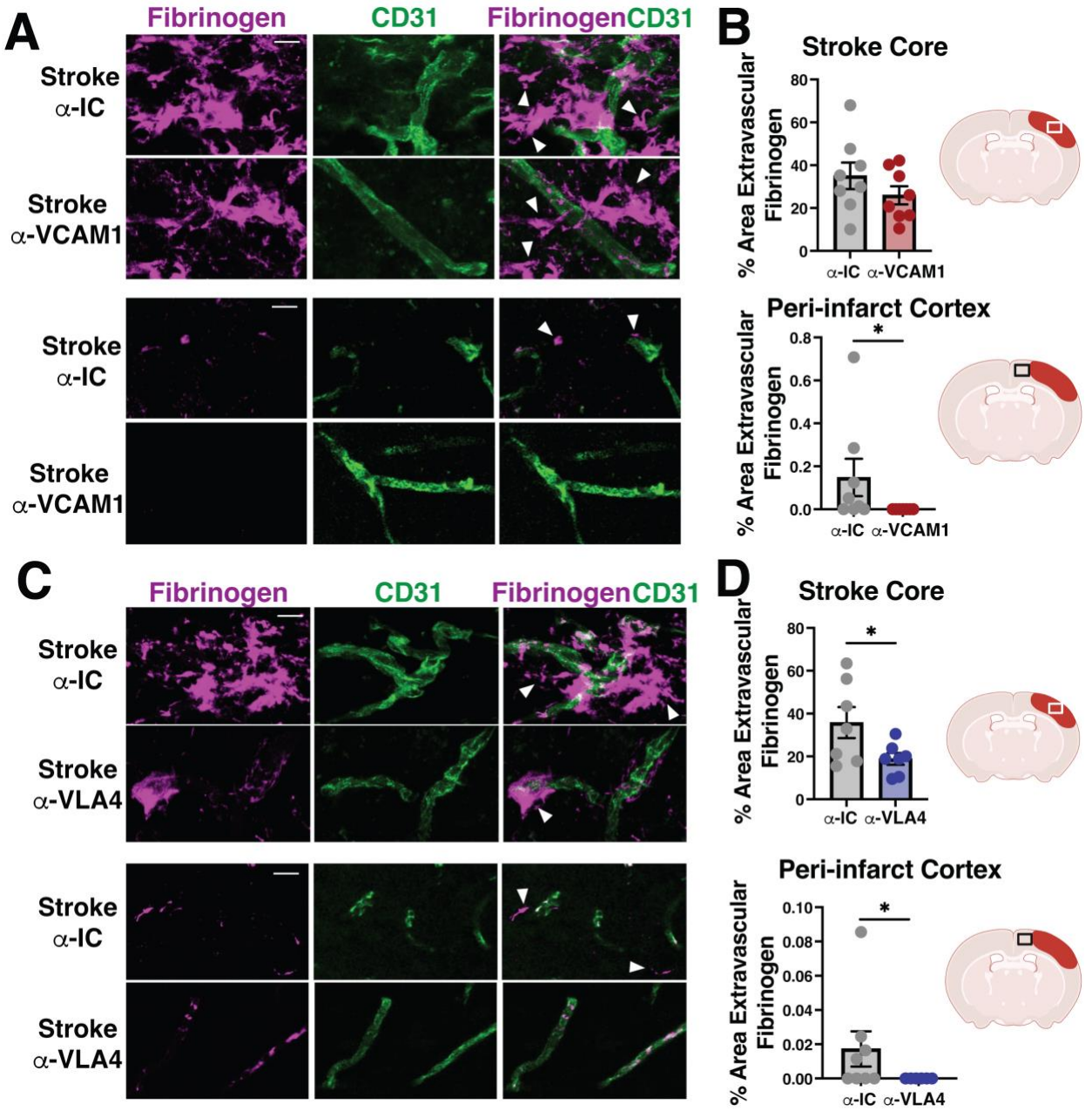

Figure 7. Anti-VCAM1 and anti-VLA4 chronic treatment reduces blood-brain barrier leakage. A) Representative confocal images and B) quantification of the percent area covered by extravascular fibrinogen in the stroke core (top) and peri-infarct cortex (bottom) of mice treated with chronic isotype control (Stroke-α-IC) or anti-VCAM1 (Stroke-α-VCAM1) antibody for 3 weeks. C) Representative confocal images and D) quantification of the percent area covered by extravascular fibrinogen in the stroke core (top) and peri-infarct cortex (bottom) of mice treated with chronic isotype control (Stroke-α-IC) or anti-VLA4 (Stroke-α-VLA4) antibody for 3 weeks. White arrows point to extravascular fibrinogen. Scale bar, 20 μM; Statistics, Student's *t* test; Error bars, mean ± SEM; *$p < 0.05$.

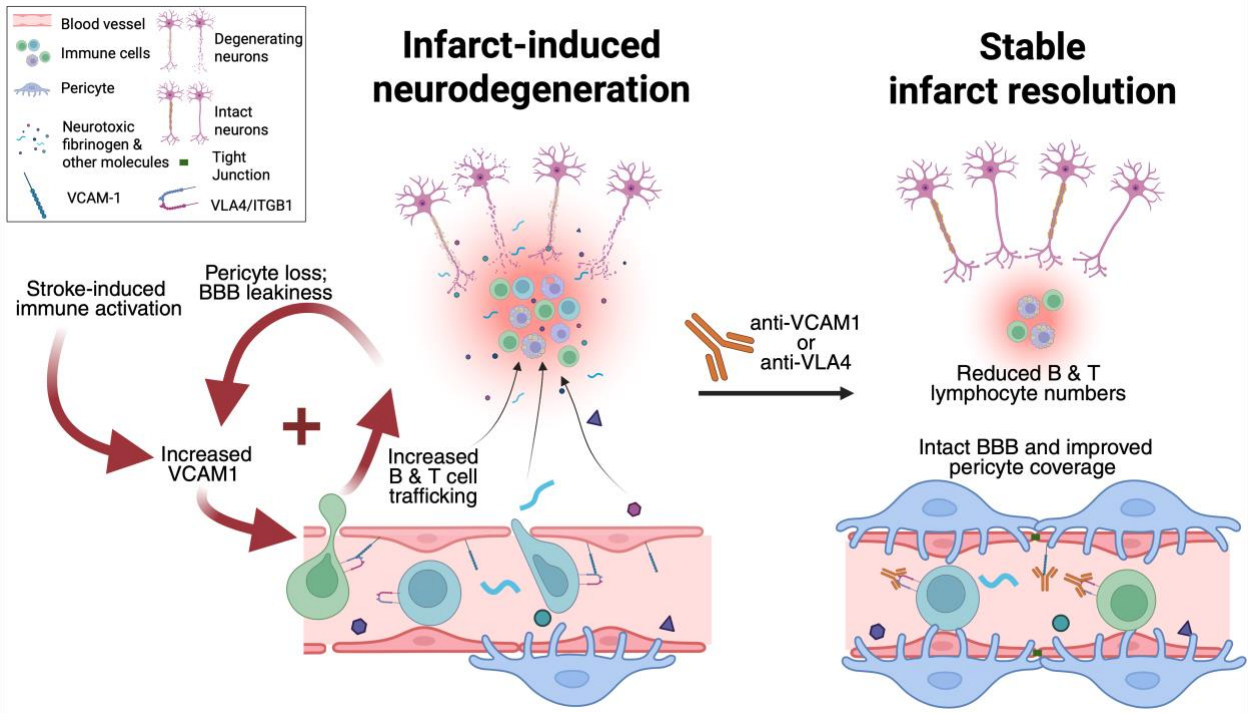

Figure 8. Proposed mechanism of the VCAM1/VLA4 axis in preventing infarct-induced neurodegeneration. The diagram depicts our proposed hypothesis of how infarct-induced neurodegeneration, a chronic process, can be prevented with chronic blockade of the VLA4/VCAM1 axis. We propose that infarct-induced neurodegeneration occurs when the initial inflammation due to stroke fails to resolve, resulting in chronic immune cell trafficking to the brain, chronic blood-brain barrier leakiness and subsequent cognitive decline. Chronic blockade of the VLA4/VCAM1 signaling axis restores blood-brain barrier integrity, reduces immune cell trafficking to the brain, and prevents chronic cognitive decline after stroke. Diagram created using BioRender.

Supplemental Data:

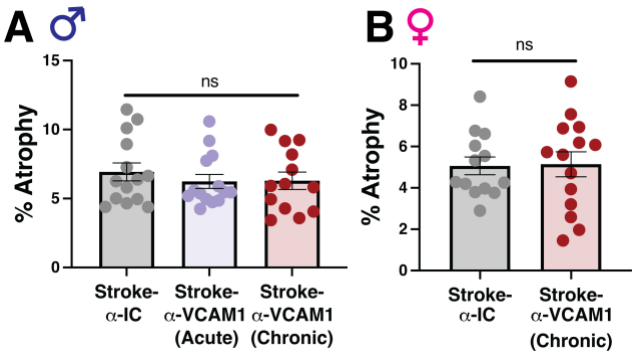

Supplementary Figure 1. Chronic brain atrophy is unchanged by anti-VCAM1 treatment in middle-aged mice. Quantification of total brain atrophy in 10 month old male (A) or female (B) mice. Mice were treated with isotype control (Stroke-α-IC; n=14 male, n=13 female) or anti-VCAM1 (Stroke-α-VCAM1) antibody acutely (n=14 male) or chronically (n=13 male, n=14 female. Statistics, Student's *t* test or one-way ANOVA with Tukey's post-hoc test; Error bars, mean ± SEM.

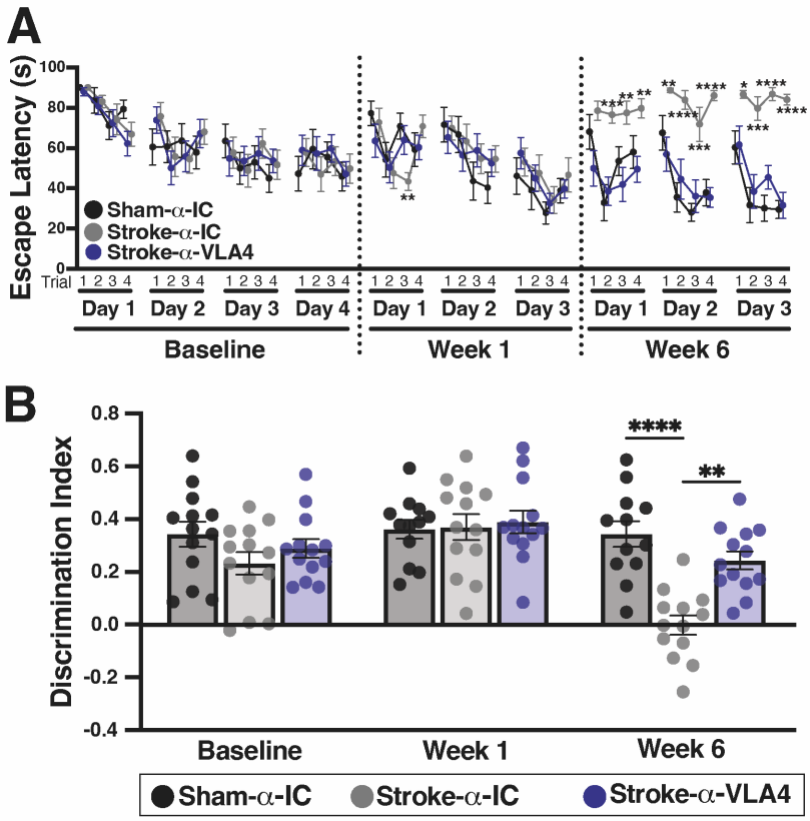

Supplementary Figure 2. Anti-VLA4 chronic antibody treatment prevents cognitive decline in middle-aged female mice. A) Escape latency on the Barnes maze and B) discrimination index on the novel object recognition task for 10 month old female mice treated with isotype control antibody (α-IC; n=13 sham and 13 stroke or anti-VLA4 (α-VLA4; n=13) chronically. Statistics, 2-way repeated measures ANOVA with Bonferroni's post-hoc test; Error bars, mean ± SEM; *p < 0.05; **p < 0.01; ***p < 0.001; ****p < 0.0001.

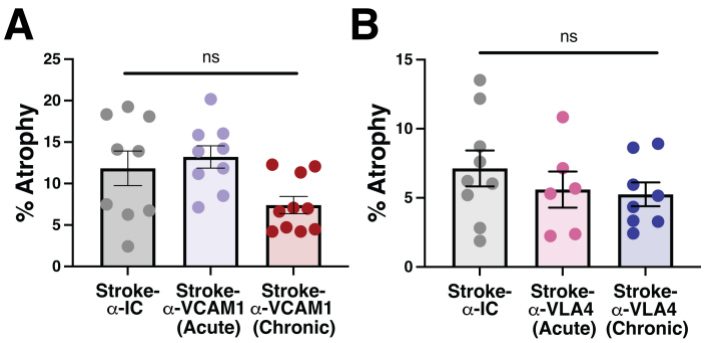

Supplementary Figure 3. Chronic brain atrophy is unchanged by anti-VCAM1 or anti-VLA4 treatment in adult mice. Quantification of total brain atrophy in 3 month old male mice. In (A), mice were treated with isotype control (Stroke-α-IC; n=9) or anti-VCAM1 (Stroke-α-VCAM1) antibody acutely (n=9) or chronically (n=10) for 3 weeks. In (B) mice were treated with isotype control (Stroke-α-IC; n=9) or anti-VLA4 (Stroke-α-VLA4) antibody acutely (n=6) or chronically (n=8). Statistics, one-way ANOVA with Tukey's post-hoc test; Error bars, mean ± SEM.

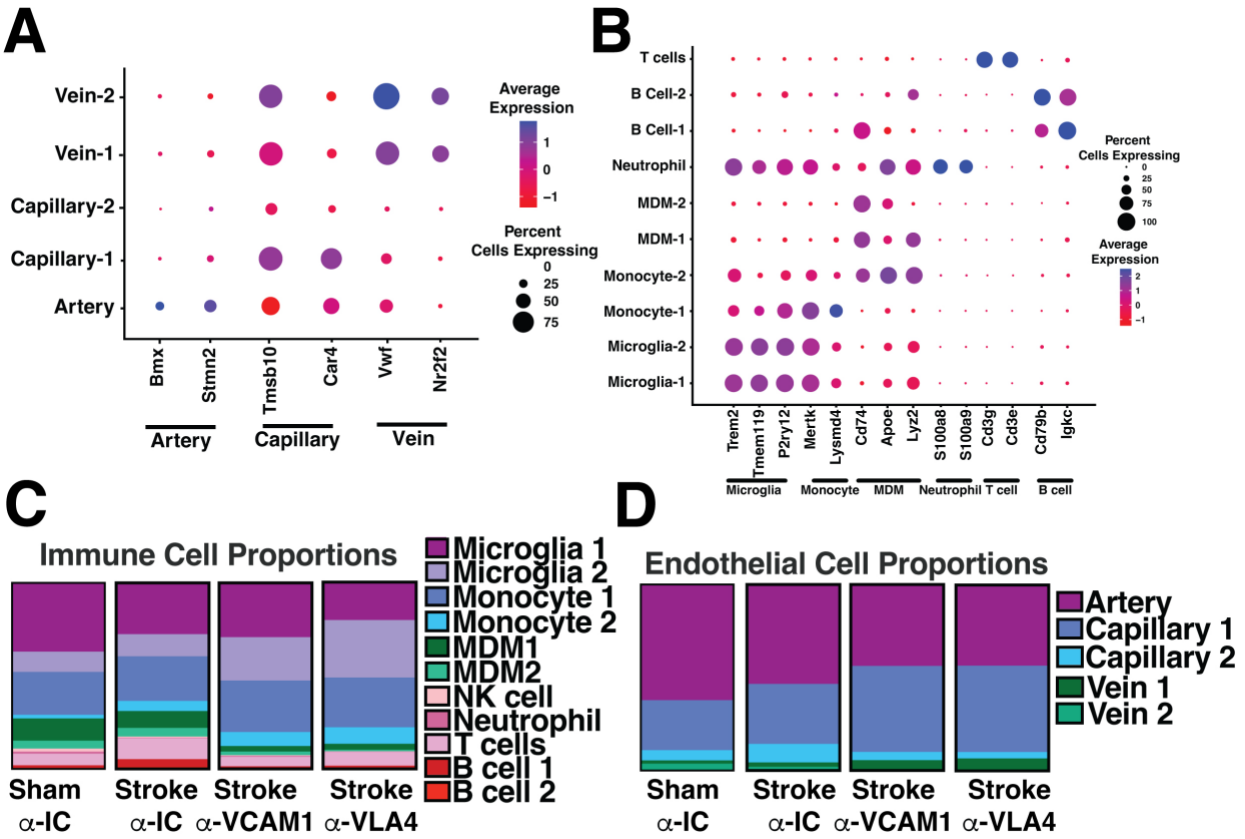

Supplementary Figure 4. Chronic anti-VCAM1 and anti-VLA4 treatment does not alter immune cell phenotype chronically after stroke. A dotplot of cell marker genes was used to annotate cell clusters in (A) endothelial and (B) immune cells. A graphical representation of the proportion of cells collected from each cluster, separated by sample for immune (C) and endothelial (D) cells.

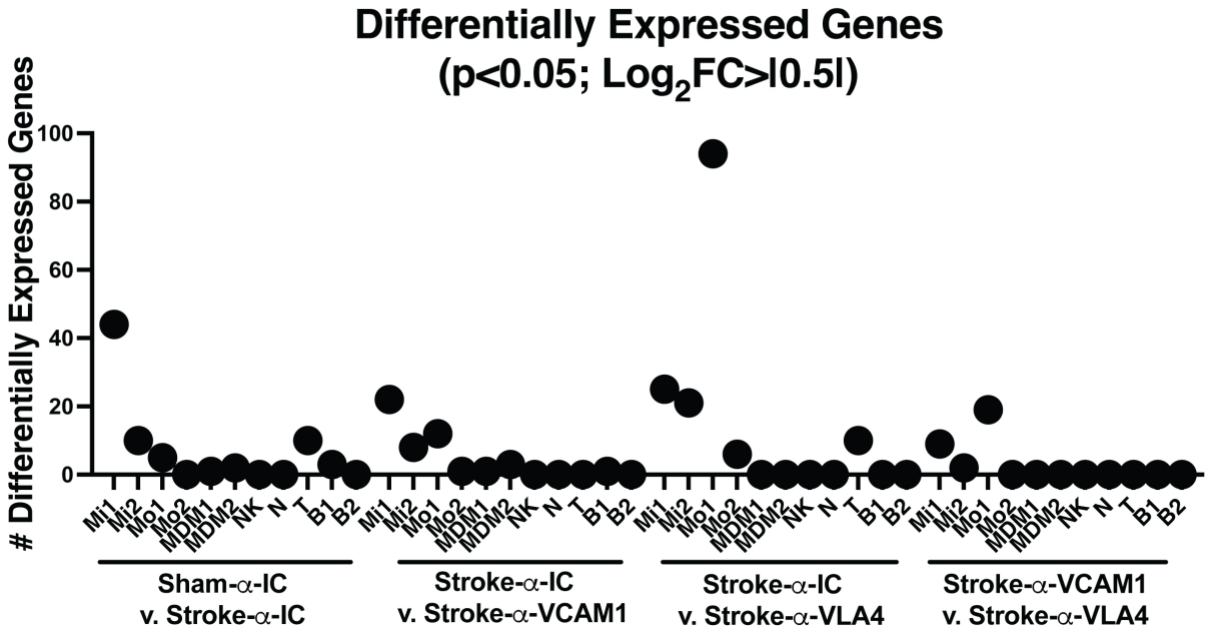

Supplementary Figure 5. A graphical representation of the number of differentially expressed genes in immune cell subpopulations defined by $p<0.05$ and $Log_2FoldChange>|0.5|$. Mi, Microglia; Mo, Monocyte; MDM, Monocyte-derived macrophage; NK, Natural Killer cell; N, Neutrophil; T, T cell; B, B cell.

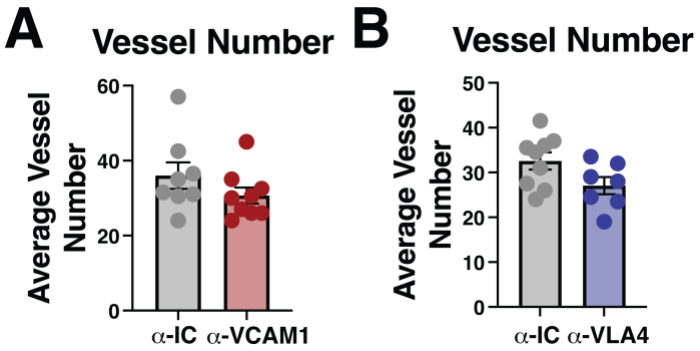

Supplementary Figure 6. Total vessel number is unchanged after chronic anti-VCAM1 or anti-VLA4 treatment. Quantification of total blood vessel number in 3 month old male mice. In (A), mice were treated with isotype control (α-IC, n=8) or anti-VCAM1 (α-VCAM1) antibody (n=9) every 3 days for 3 weeks. In (B) mice were treated with isotype control (α-IC, n=9) or anti-VLA4 (α-VLA4, n=7) antibody every 3 days for 3 weeks. Statistics, Student's *t* test; Error bars, mean ± SEM.

Supplementary Table 1. Cell markers used to annotate clusters isolated during single cell RNA sequencing of CD45+ and CD31+ cells. We isolated CD31+ endothelial and CD45+ immune cells from the stroke scar of 10 month old male C57BL/6J mice, 10 weeks after stroke or sham surgery. We used the UMAP algorithm to independently cluster each cell type by similarity and utilized cell-specific markers to annotate the resulting clusters.

Dataset	Cell Sub-type	Marker	Reference(s)Figure 1B
CD31	Artery	*Stmn2*	(42, 59)
		Bmx	(42, 59)
CD31	Capillary	*Tmsb10*	(42, 59)
		Car4	(42, 59)
CD31	Vein	*Vwf*	(42, 59)
		Nr2f2	(42, 59)
CD45	Microglia	*Tmem119*	(60)
		Trem2	(60)
		P2ry12	(60)
CD45	Monocyte	*Mertk*	(61)
		Lysmd4	(61)
CD45	Monocyte-derived Macrophage	*Apoe*	(61)
		Lyz2	(61)
		Cd74	(61)
CD45	Neutrophil	*S100a8*	(37)
		S100a9	(37)
CD45	T cell	*Cd3g*	(61)
		Cd3e	(61)
CD45	B cell	*Igkc*	(37)
		Cd79b	(37)

Supplementary Table 2. Plasma protein concentrations from SomaLogic Proteomics. We measured the concentration of 5,284 proteins from the plasma with SomaLogic Proteomics. Mice were 10 month old males and treated with IgG or anti-VCAM1 chronically until 10 weeks after stroke. We used a Mann Whitney U Test to determine whether protein concentrations were altered by antibody treatment. A univariate Spearman correlation was performed to analyze the relationship between protein concentration, regardless of treatment group, and cognitive function. To assess cognitive function, a cognitive score was calculated by averaging the Barnes Maze performance from trials 3 & 4 of the final day of testing for each mouse. Here, a lower cognitive score represents better cognitive function.

Protein Symbol	**Protein Name**	**Protein Concentrations**		**Correlation with Barnes Maze performance**	
		IgG: VCAM1 Ratio	**Mann Whitney P value**	**Spearman rho**	**Spearman P value**

References

1. Ivan CS, et al. Dementia after stroke: the Framingham Study. *Stroke*. 2004;35(6):1264–1268.

2. Doyle KP, Buckwalter MS. Immunological mechanisms in poststroke dementia. *Curr Opin Neurol*. 2020;33(1):30–36.

3. Doyle KP, Buckwalter MS. Does B lymphocyte-mediated autoimmunity contribute to post-stroke dementia? *Brain Behav Immun*. 2017;64:1–8.

4. Feigin VL, et al. World stroke organization (WSO): Global Stroke Fact Sheet 2022. *Int J Stroke*. 2022;17(1):18–29.

5. Brainin M, et al. Post-stroke cognitive decline: an update and perspectives for clinical research. *Eur J Neurol*. 2015;22(2):229–38, e13-6.

6. Mijajlović MD, et al. Post-stroke dementia - a comprehensive review. *BMC Med*. 2017;15(1):11.

7. Pollock A, et al. Top 10 research priorities relating to life after stroke--consensus from stroke survivors, caregivers, and health professionals. *Int J Stroke*. 2014;9(3):313–320.

8. McKevitt C, et al. Self-reported long-term needs after stroke. *Stroke*. 2011;42(5):1398–1403.

9. Wolfe CDA, et al. Estimates of outcomes up to ten years after stroke: analysis from the prospective South London Stroke Register. *PLoS Med*. 2011;8(5):e1001033.

10. Corraini P, et al. Long-term risk of dementia among survivors of ischemic or hemorrhagic stroke. *Stroke*. 2017;48(1):180–186.

11. Manwani B, et al. Functional recovery in aging mice after experimental stroke. *Brain Behav Immun*. 2011;25(8):1689–1700.

12. El Husseini N, et al. Cognitive impairment after ischemic and hemorrhagic stroke: A scientific statement from the American heart association/American stroke association. *Stroke*. 2023;54(6):e272–e291.

13. Doyle KP, et al. B-lymphocyte-mediated delayed cognitive impairment following stroke. *J Neurosci*. 2015;35(5):2133–2145.

14. Filippi M. Mechanism of diapedesis: Importance of the transcellular route. *Adv Immunol*. 2016;129:25–53.

15. Schoppmeyer R, van Buul JD. The diapedesis synapse: dynamic leukocyte-endothelium interactions. *Curr Opin Physiol*. 2021;19:1–9.

16. Elkind MSV, et al. Natalizumab in acute ischemic stroke (ACTION II). *Neurology*. 2020;95(8):e1091–e1104.

17. Elkins J, et al. Safety and efficacy of natalizumab in patients with acute ischaemic stroke (ACTION): a randomised, placebo-controlled, double-blind phase 2 trial. *Lancet Neurol*. 2017;16(3):217–226.

18. Yousef H, et al. Aged blood impairs hippocampal neural precursor activity and activates microglia via brain endothelial cell VCAM1. *Nat Med*. 2019;25(6):988–1000.

19. Doyle KP, et al. Distal hypoxic stroke: a new mouse model of stroke with high throughput, low variability and a quantifiable functional deficit. *J Neurosci Methods*. 2012;207(1):31–40.

20. Wilson EN, et al. TREM1 disrupts myeloid bioenergetics and cognitive function in aging and Alzheimer disease mouse models. *Nat Neurosci*. 2024;27(5):873–885.

21. Lechtenberg KJ, et al. Augmented β2-adrenergic signaling dampens the neuroinflammatory response following ischemic stroke and increases stroke size. *J Neuroinflammation*.

2019;16(1):112.

22. Xie Z, et al. Gene set knowledge discovery with Enrichr. *Curr Protoc*. 2021;1(3):e90.

23. Kuleshov MV, et al. Enrichr: a comprehensive gene set enrichment analysis web server 2016 update. *Nucleic Acids Res*. 2016;44(W1):W90-7.

24. Chen EY, et al. Enrichr: interactive and collaborative HTML5 gene list enrichment analysis tool. *BMC Bioinformatics*. 2013;14:128.

25. Llovera G, et al. Results of a preclinical randomized controlled multicenter trial (pRCT): Anti-CD49d treatment for acute brain ischemia. *Sci Transl Med*. 2015;7(299):299ra121.

26. Relton JK, et al. Inhibition of α4 integrin protects against transient focal cerebral ischemia in normotensive and hypertensive rats. *Stroke*. 2001;32(1):199–205.

27. Langhauser F, et al. Blocking of α4 integrin does not protect from acute ischemic stroke in mice. *Stroke*. 2014;45(6):1799–1806.

28. Becker K, et al. Antibody to the α4 integrin decreases infarct size in transient focal cerebral ischemia in rats. *Stroke*. 2001;32(1):206–211.

29. Liesz A, et al. Inhibition of lymphocyte trafficking shields the brain against deleterious neuroinflammation after stroke. *Brain : a journal of neurology*. 2011;134 Pt 3:704–720.

30. Mindur JE, et al. Early treatment with anti-VLA-4 mAb can prevent the infiltration and/or development of pathogenic CD11b+CD4+ T cells in the CNS during progressive EAE. *PLoS One*. 2014;9(6):e99068.

31. Yednock TA, et al. Prevention of experimental autoimmune encephalomyelitis by antibodies against alpha 4 beta 1 integrin. *Nature*. 1992;356(6364):63–66.

32. Pyka-Fościak G, Lis GJ, Litwin JA. Adhesion molecule profile and the effect of anti-VLA-4 mAb treatment in experimental autoimmune encephalomyelitis, a mouse model of multiple sclerosis. *Int J Mol Sci*. 2022;23(9):4637.

33. Deloire MSA, et al. Macrophage brain infiltration in experimental autoimmune encephalomyelitis is not completely compromised by suppressed T-cell invasion: in vivo magnetic resonance imaging illustration in effective anti-VLA-4 antibody treatment. *Mult Scler*. 2004;10(5):540–548.

34. Zhang S, et al. Macrophage-mediated vascular permeability via VLA4/VCAM1 pathway dictates ascites development in ovarian cancer. *J Clin Invest*. 2021;131(3). https://doi.org/10.1172/JCI140315.

35. García-Martín AB, et al. VLA-4 mediated adhesion of melanoma cells on the blood-brain barrier is the critical cue for melanoma cell intercalation and barrier disruption. *J Cereb Blood Flow Metab*. 2019;39(10):1995–2010.

36. van Wetering S, et al. VCAM-1-mediated Rac signaling controls endothelial cell-cell contacts and leukocyte transmigration. *Am J Physiol Cell Physiol*. 2003;285(2):C343-52.

37. Zheng K, et al. Single-cell RNA-seq reveals the transcriptional landscape in ischemic stroke. *J Cereb Blood Flow Metab*. 2022;42(1):56–73.

38. Garcia-Bonilla L, et al. Analysis of brain and blood single-cell transcriptomics in acute and subacute phases after experimental stroke. *Nat Immunol*. 2024;25(2):357–370.

39. Marsh SE, et al. Dissection of artifactual and confounding glial signatures by single-cell sequencing of mouse and human brain. *Nat Neurosci*. 2022;25(3):306–316.

40. Becker KJ, et al. Antibodies to myelin basic protein are associated with cognitive decline after

stroke. *J Neuroimmunol*. 2016;295–296:9–11.

41. Becker KJ, et al. Autoimmune responses to the brain after stroke are associated with worse outcome. *Stroke*. 2011;42(10):2763–2769.

42. Chen MB, et al. Brain Endothelial Cells Are Exquisite Sensors of Age-Related Circulatory Cues. *Cell Rep*. 2020;30(13):4418-4432.e4.

43. Wei L, et al. Collateral growth and angiogenesis around cortical stroke. *Stroke*. 2001;32(9):2179–2184.

44. Bowman GL, et al. Blood-brain barrier breakdown, neuroinflammation, and cognitive decline in older adults. *Alzheimers Dement*. 2018;14(12):1640–1650.

45. Hussain B, Fang C, Chang J. Blood-brain barrier breakdown: An emerging biomarker of cognitive impairment in normal aging and dementia. *Front Neurosci*. 2021;15:688090.

46. Barisano G, et al. Blood-brain barrier link to human cognitive impairment and Alzheimer's Disease. *Nat Cardiovasc Res*. 2022;1(2):108–115.

47. Petersen MA, Ryu JK, Akassoglou K. Fibrinogen in neurological diseases: mechanisms, imaging and therapeutics. *Nat Rev Neurosci*. 2018;19(5):283–301.

48. Merlini M, et al. Fibrinogen induces microglia-mediated spine elimination and cognitive impairment in an Alzheimer's disease model. *Neuron*. 2019;101(6):1099-1108.e6.

49. Ryu JK, et al. Fibrin-targeting immunotherapy protects against neuroinflammation and neurodegeneration. *Nat Immunol*. 2018;19(11):1212–1223.

50. Adams RA, et al. The fibrin-derived gamma377-395 peptide inhibits microglia activation and suppresses relapsing paralysis in central nervous system autoimmune disease. *J Exp Med*.

2007;204(3):571–582.

51. Shabani Z, et al. Increased synapse elimination by inflammatory cells contributes to long-lasting post-stroke memory dysfunction in old mice. *bioRxiv*. 2025. https://doi.org/10.1101/2025.06.13.659591.

52. Li Z, et al. Fracture shortly before stroke in mice leads to hippocampus inflammation and long-lasting memory dysfunction. *J Cereb Blood Flow Metab*. 2020;40(2):446–455.

53. Khan R, et al. Neuropathological hallmarks during the chronic phase of ischemic stroke in mice and humans. *bioRxiv*. 2025. https://doi.org/10.1101/2025.04.16.649173.

54. Li P, Fan H. Pericyte Loss in Diseases. *Cells*. 2023;12. https://doi.org/10.3390/cells12151931.

55. Fernández-Klett F, et al. Early loss of pericytes and perivascular stromal cell-induced scar formation after stroke. *J Cereb Blood Flow Metab*. 2013;33(3):428–439.

56. Castillo-González J, González-Rey E. Beyond wrecking a wall: revisiting the concept of blood-brain barrier breakdown in ischemic stroke. *Neural Regen Res*. 2025;20(7):1944–1956.

57. Liang Y, et al. Blood-brain barrier disruption and imaging assessment in stroke. *Transl Stroke Res*. [published online ahead of print: September 25, 2024]. https://doi.org/10.1007/s12975-024-01300-6.

58. Candelario-Jalil E, Dijkhuizen RM, Magnus T. Neuroinflammation, stroke, blood-brain barrier dysfunction, and imaging modalities. *Stroke*. 2022;53(5):1473–1486.

59. Berthiaume A-A, et al. Pericyte remodeling is deficient in the aged brain and contributes to impaired capillary flow and structure. *Nat Commun*. 2022;13(1):5912.

60. Yang AC, et al. Physiological blood-brain transport is impaired with age by a shift in

transcytosis. *Nature*. 2020;583(7816):425–430.

61. Mattioli F, et al. Natalizumab Significantly Improves Cognitive Impairment over Three Years in MS: Pattern of Disability Progression and Preliminary MRI Findings. *PLoS One*. 2015;10(7):e0131803.

62. Soon D, et al. A study of subtle blood brain barrier disruption in a placebo-controlled trial of natalizumab in relapsing remitting multiple sclerosis. *J Neurol*. 2007;254(3):306–314.

63. Cramer SP, et al. Permeability of the blood-brain barrier in normal appearing white and grey matter predicts early inadequate treatment response to fingolimod og natalizumab. *MULTIPLE SCLEROSIS JOURNAL*. SAGE PUBLICATIONS LTD 1 OLIVERS YARD, 55 CITY ROAD, LONDON EC1Y 1SP, ENGLAND; 2016:669–670.

64. Lang C, Reiss C, Mäurer M. Natalizumab may improve cognition and mood in multiple sclerosis. *Eur Neurol*. 2012;67:162–166.

65. Perumal J, et al. Improvements in Cognitive Processing Speed, Disability, and Patient-Reported Outcomes in Patients with Early Relapsing-Remitting Multiple Sclerosis Treated with Natalizumab: Results of a 4-year, Real-World, Open-Label Study. *CNS Drugs*. 2022;36(9):977–993.